COMPUTATIONAL INVESTIGATION OF FLOW FIELDS AND DETAILED CHEMISTRY IMPACTS ON IGNITION DELAYS

A Thesis
Presented to
The Academic Faculty

By

David B. Ritter

Of the Requirements for the Degree
Masters of Science in the
George W. Woodruff School of Mechanical Engineering

Georgia Institute of Technology
August 2020

COMPUTATIONAL INVESTIGATION OF FLOW FIELDS AND DETAILED CHEMISTRY IMPACTS ON IGNITION DELAYS

Approved by:

Dr. Wenting Sun, Advisor
The Daniel Guggenheim School of Aerospace Engineering
Georgia Institute of Technology

Dr. Caroline Genzale
The Daniel Guggenheim School of Mechanical Engineering
Georgia Institute of Technology

Dr. Timothy Lieuwen
George W. Woodruff School of Mechanical Engineering
Georgia Institute of Technology

Dr. Vaidya Sankaran
AIAA Associate Fellow
Pratt & Whitney

Date Approved: July 22, 2020

ACKNOWLEDGEMENTS

Thanks to my family, Liz, Barry, & Tina, for the constant support throughout this project and degree. Thank you Carrie for the love and encouragement. I would also like to thank the Raytheon Technology Employee Scholar Program for funding this degree, Pratt & Whitney's high performance computing for computational resources, and guidance & feedback from coworkers.

TABLE OF CONTENTS

LIST OF TABLES

LIST OF FIGURES

LIST OF ACRONYMS

CFD	Computational Fluid Dynamics
CR	Compression Ratio
DES	Detached Eddy Simulation
DTI	Dual Time-step Integration
EDC	Eddy-Dissipation Concept
EDC	Eddy-Dissipation Concept
EGR	Exhaust Gas Recirculation
HCCI	Homogeneous-Charge Compression Ignition
IC	Internal Combustion
ID	Inner Diameter
ISAT	In Situ Adaptive Tabulation
KE	K- Epsilon
LES	Large Eddy Simulation
LTC	Low Temperature Chemistry
OD	Outer Diameter
RANS	Reynolds Averaged Navier-Stokes
RCM	Rapid Compression Machines
SBES	Stress-Blending Eddy Simulation
SST	Shear Stress Transport
TCI	Turbulent Chemistry Interaction
TDC	Top Dead Center
UDF	User-Defined Function
WALE	Wall-Adapting Local Eddy-viscosity

SUMMARY

This work investigated the impacts of a complex piston head geometry on the aerodynamics and chemical kinetics in a Rapid Compression Machine. Utilizing 2D axisymmetric Computational Fluid Dynamics, a single stage compression and ignition was simulated for three different piston head geometries. The numeric framework resolved the flow structures through a hybrid RANS–LES model, and simulated the reaction with a diluted 29 species, 52 equation reduced global mechanism for n-heptane. The hybrid viscosity model was found to provide excellent qualitative information regarding the aerodynamic structures within a reasonable run time. Differences across geometry in vortex formation and interaction with the piston is presented. Negligible differences in global temperature or ignition delay were observed for the different piston geometries. The variable piston geometry was found to highly impact the cold roll up vortex, alter the chemical reaction pathways and acoustic resonance in the fluid domain. Geometric features were identified as possible alternative solutions to vortex mitigation compared to other strategies currently used in RCMs.

Chapter 1: Introduction

Rapid Compression Machines (RCM) have a long history as effective test vehicles for experimental combustion at Internal Combustion conditions. Specifically used for studying chemical kinetics, RCMs provide a test vehicle for easily compressing fuel and timing pressure rise to measure the combustibility of various fuels at a wide range of conditions. In current studies of chemical kinetics understanding the pathways and properly fitting models is paramount for reduced computational complexity while resolving fine kinetics.

Early RCMs were identified as being effective tools to characterizing ignition delays [1]. Shock tubes are also able to simulate a wide range of conditions however are more transient in nature, whereas RCMs can maintain compressed conditions an order of magnitude longer [2]. Benefits in studying chemical kinetics in RCMs over reciprocating engines include simplifying to a single stage compression negating cycle to cycle variation [3] and drastically reduced fuel costs [1].

There are some drawbacks of RCMs, such as mechanical difficulties due to high piston velocities coming to rapid stops and heat loss through the system [1]. Differences in early RCM testing between measured results and ideal compression was hypothesized to be driven by heat loss from the system [1]. Increased heat loss was found to be a result of the cold roll up phenomena identified by Daneshyar et al. showing both laminar and turbulent structures generated through piston compression using dye-vis [3]. These structures are generated by the piston shearing the cold boundary layer formed on the cylinder wall entraining warm air in a cold gas vortex. While identified as applicable to all Internal Combustion (IC) cycles this was found

to have a minimal impact at fast engine operations for common IC applications [3] and thus became a more central topic in the study of RCMs. Cold roll up vortices are unsteady in nature due to the short compression time and can have drastic and varying impacts. Work by Sung et al highlighted the variability in generated vortices in RCMs highlighting the importance of fully simulating the compression stroke when studying ignition delays [2]. This is especially apparent due to the sensitivity of the roll up to fluctuations of the piston velocity during compression [4].

Griffiths et al. presented early Computational Fluid Dynamics (CFD) simulation coupling flow characterization and kinetic modeling which accurately simulated of the cold roll up vortex and confirmed that regions outside the roll up see adiabatic compression [5]. Prior, 1D thermo-chemical were able to decently simulate RCMs but required numeric increments to match results [5]. Further CFD implementation work by Chen and Karim assessed important modeling decision (such as initial conditions, compression ratio, and elemental diluent parameters) and found fair agreement between models and experiments [6]. An interesting finding was the competition between local impacts of the cold roll up, which accelerated ignition, and the overall increased rate of heat loss to the ambient which hindered the kinetics on a macro level [6].

Given the prevalence of chemical kinetics studies in RCMs, producing a uniform flow field reduces additional variable in interrogating RCM data and producing representative models. A cut out plenum in the piston first [7] proposed by Park and Keck, called a “Crevice”, was found to successfully capture most of the cold gas and largely mitigate vortex generation [8]. Sung and Curran concluded that studies with crevice implementation can accurately predict the first ignition, however are less accurate for later kinetic spans after a large heat release [2]. Lee

and Hochgreb expanded successful crevice implementation through an equation based model and produced a uniform thermal field [9]. Work utilizing CFD was completed by Mittal et al to study the crevice, specifically looking at optimal sizing and different modeling techniques [10] [11]. Studies of non-standard RCM configurations by Wurmel and Simmie studied crevice optimization and found an effective double piston head configuration for uniform flow fields after compression however were unable to completely abate the cold roll up structures [12].

Crevice technology development is important since it improves the ability to smooth out flow and reduce thermo-kinetic variables but also include drawbacks which drive additional computational and configuration complexity. One issue with crevice implementation is effectively partitioning the flow once the reaction begins [13]; contamination across the two regions can negate the benefits of roll up capture. Absolute mitigation is also unachieved as in many works the roll up is not completely abated and non-uniformities still exist after compression [10] [11] [12] [13].

Alterations to IC's (and thus RCM's) chambers and pistons to manipulate combustion have been employed extensively in the past. A well-known alteration in trucks is a hemispheric dome and piston which alters the ratio of volume to surface area and changing intake charge characteristics. Alterations to the piston have looked at thermal coatings to alter heat transfer between the piston and gas volume [14]. Efforts to control turbulent flow structures include channels cut into the cylinder head, called "squish" features, which route air into small channels increasing turbulent mixing prior and during combustion to reduce emissions and Nitrogen Oxides (NOx) [15]. A CFD study by Harshavardhan and Mallikarjuna looked at turbulence

effects in direct injection spark ignition due to variable piston geometry, and found a negative bowl feature increased turbulent kinetic energy in the gas domain and increased fuel evaporation [16].

The goal of this project is to investigate the flow and kinetic impacts on cold roll up structures of different piston geometries. Past work highlights the importance of chemical kinetics and the benefits of a uniform flow field. Since prevention of these structures is not fully possible, understanding their impacts is important. The impacts of the flow structures will be studied by altering the piston geometry to create different flow structures and assess their relative differences on the reaction. The scope of this project includes building a 2D axisymmetric (CFD) model and executing a small design of experiments testing a few piston head geometries. This model considered complex kinetic interactions to simulate auto-ignition and refined flow though high fidelity viscosity models.

Chapter 2: Numerical Framework

The validity of any CFD based work is in the assumptions and sub models utilized to capture the physics. The physical side relies on the characterization of turbulence and chemical kinetics through various models. On the numeric side the time step and iteration drive both stability and accuracy of the results. These two topics are interconnected, finer resolution of flow structures and reactions drive smaller time steps to capture the scales accurately, smaller time steps drive lower iterations etc and computational time. To understand these models and increase confidence in the results many submodels and sensitivities were executed to substantiate the studies framework. To investigate the physical models, a homogeneous reactive sub-model was built using CFD to test various turbulent and chemical models, and identified a combination that matched Chemkin [17] simulations. To determine numeric settings, time and grid independence sensitivity studies were leveraged to find the optimal lengths.

2.1 Chemical Kinetic Model

The n-heptane model selected is Patel, Kong, & Reitz's 29 species, 52 reaction model [18]. This mechanism was developed by analyzing reactions pathways in SENKIN [19] and identifying opportunities to stream line the reactions to represent different sub pathways through tuning reaction constants [18]. The mechanism was validated against HCCI simulations of more complex and established mechanisms, such as Lawrence Livermore National Lab's (LLNL) n-heptane model which considers hundreds of radicals and thousands of reactions [20], which was shown to track closely at reduced computational cost [18]. The reduced mechanism was adapted from simulations of a broad range of initial conditions for temperature (550 – 1700 K), pressure

(1 – 42 atm) and equivalence ratio (0.3 – 1.5) [18], which will bound cases in this study. The model was adapted from cases with a lower level of diluent, however the model was validated against an Exhaust Gas Recirculation (EGR) of roughly 30% [18] which is on the order of cases that will be investigated in this work. Homogeneous-Charge Compression Ignition (HCCI) is a slightly different physical IC problem than an RCM as it includes an intake charge however, the reliance on auto ignition required the same kinetics seen in an RCM. The computational load of 29 species is also found to be an acceptable cost going forward. Other models, such as LLNLs Detailed Mechanism 3.1 [20] and a larger 58 species reduced mechanism presented by Yoo et al [21], were assessed in preliminary phases of this project however were not utilized due to the incredible computational strain associated with increased number of species and reactions.

As presented in previous work, studying ignition delay with an inert diluent such, as Argon, can extend ignition delay times and allow for detailed studying complex kinetic behavior [10], but also allows for precise measurement in time and chemical radicals during testing. Previous work found possible discrepancies in diluting chemical kinetic models with elements other than the model was tuned with [6], however only accounted for negligible changes.

2.2 Closed Homogenous Solver – Viscosity Model

To investigate the physical models, a homogeneous reaction sub-model was built using CFD to test various turbulent and chemical models, and identified a combination that matched 0D Chemkin results. This work looked to assess kinetic pathways so used lower dimensional model results as a starting point to ensure no numeric diffusion was added through other models used in the solution.

This project has chosen to use ANSYS Chemkin 2019R2 standalone for a zero dimensional solver as a reference. This was used as it is the platform integrated in Fluent so shares common chemical mechanism input files, and is readily available. Simple closed homogenous constant volume reactor models are commonly used for theoretical combustion problems coupling thermo-chemical interactions [22]. This model is also simple to model in CFD and strips out any complexities due to compression so is ideal for defining viscosity and reaction options. In Chemkin the "closed homogeneous reactor" model, with a fixed volume was used while solving the energy equation. For these simulations, the initial temperature, pressure, volume and initial mole fraction were input, and temperature, pressure, rate of reaction, and mole fractions were reported over time. This model will be referenced to as the zero-dimensional, 0D, here after.

A similar test problem was configured in ANSYS Fluent 2019R1. This test problem was a 2D axisymmetric representation of the air volume at Top Dead Center (TDC), with similar mesh controls to the full problem and adiabatic walls. This simplified problem, without compression or a boundary condition ignores turbulent mixing since there is no thermal gradient. This simplification is required as it is not present in the 0D model either.

Earlier stages of the project utilized a K- Epsilon (KE) turbulence scheme, aligned with other studies in the past [5], however found poor relation to 0D results. It is believed that the grid and time were finely resolved and the scheme was imposing artificial turbulent diffusion on the solution. This phenomenon was also captured by Mittal [11]. The test problem considered a

couple viscosity models, including laminar, Reynolds Averaged Navier-Stokes (RANS), Large Eddy Simulation (LES), and a Detached Eddy Simulation (DES) Scheme with Spalart-Allmaras, before finding that a hybrid K-Omega (K-ω) with LES and Stress-Blending Eddy Simulation (SBES) matched the 0D results nearly exactly, seen in Figure 1. Ultimately, near-exact alignment was found when using K-ω at two different initial temperatures (1140° shown in Figure 1, and 1450° K). Previous work found that the measured aerodynamic effects of an RCM were best captured by a laminar viscosity model [11]; this was found to have poor alignment between the test problem and Chemkin. Full characterization of the flow without a simulated model requires exact meshing on the order of the smallest magnitude length scale; this is likely to have driven the mesh to unfeasible levels.

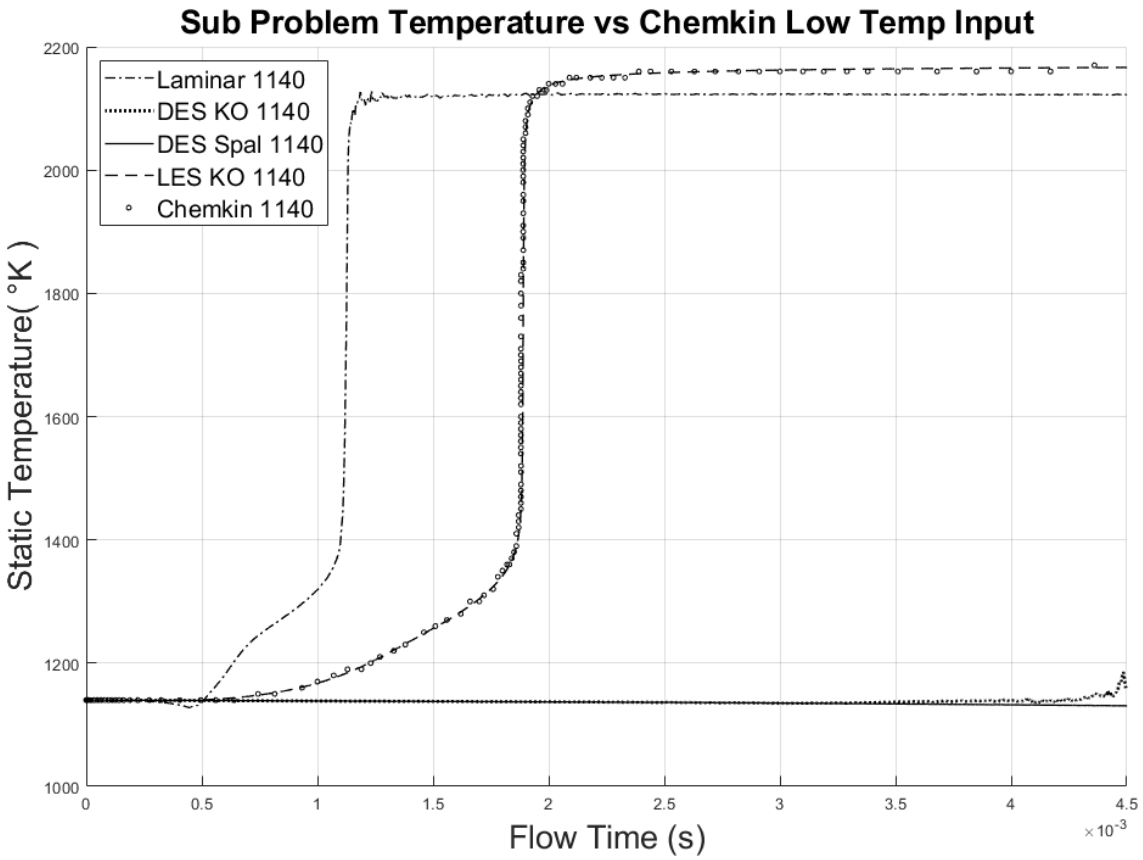

Figure 1: Viscosity Models Compared Against Chemkin Results

The standard K-ω model with shear-stress transport is a hybrid RANS model which combines KE in far field sections and K-ω near the wall [23]; this allows for a more refined wall assessment of the turbulence [23]. However, since KE was founds not desirable, the SBES functionality was selected as it utilizes Large Eddy Simulation (LES) to handle far field flow instead. LES, is a scheme which does not apply time averaging to the whole problem when solving Navier-Stokes, but instead looks to characterize large turbulent structures and approximates smaller phenomena [24]. The subgrid–scale Wall-Adapting Local Eddy-viscosity (WALE) model was chosen as this is a wall-bounded flow problem [23]. This model has the benefit of LES fidelity and intricate contours in the core of the problem but resolves the walls with 2 equations and is stable. This additional refinement required extra computational time however the main driver of solve time was the chemical kinetics so this addition was marginal.

The simple closed homogenous reactor problem was also used to test various Volumetric Reaction models and attempts to reduce computational load, however finite rate / no turbulent chemistry interaction (TCI) with stiff direct numeric integration was the only acceptable match the Chemkin results. Further assessments of numerical aids found chemistry agglomeration the only acceptable accelerator. To track individual chemical species a species transport model was used on Fluent's base platform, with an imported Chemkin reaction mechanism. Volumetric reaction was included; no spark ignition or simulated auto ignition models were used. Previously it was postulated that to handle both the intricate turbulence and complex kinetics, an Eddy-Dissipation Concept (EDC) model would be applicable [23]. As seen below in Figure 2, the Chemkin results were not matched when TCI was included. The EDC model requires turbulent fine scales to drive a reaction [23], since the simplified model assumed out sources of turbulence,

it is possible using the model drove non-physical results. This will likely not be the case in expanded complex problem, however, this is a possible flaw in bootstrapping reduced order solvers to complex problems. A postulated mitigation to the exclusion of a TCI model is the theory that if the turbulent flow structures are fully defined no additional TCI needs to be simulated. While mesh independence was determined, a possible path forward to confirm if this mesh was fine enough is to compare the current mesh with a finer mesh both running TCI; this was not completed however could be done in future work.

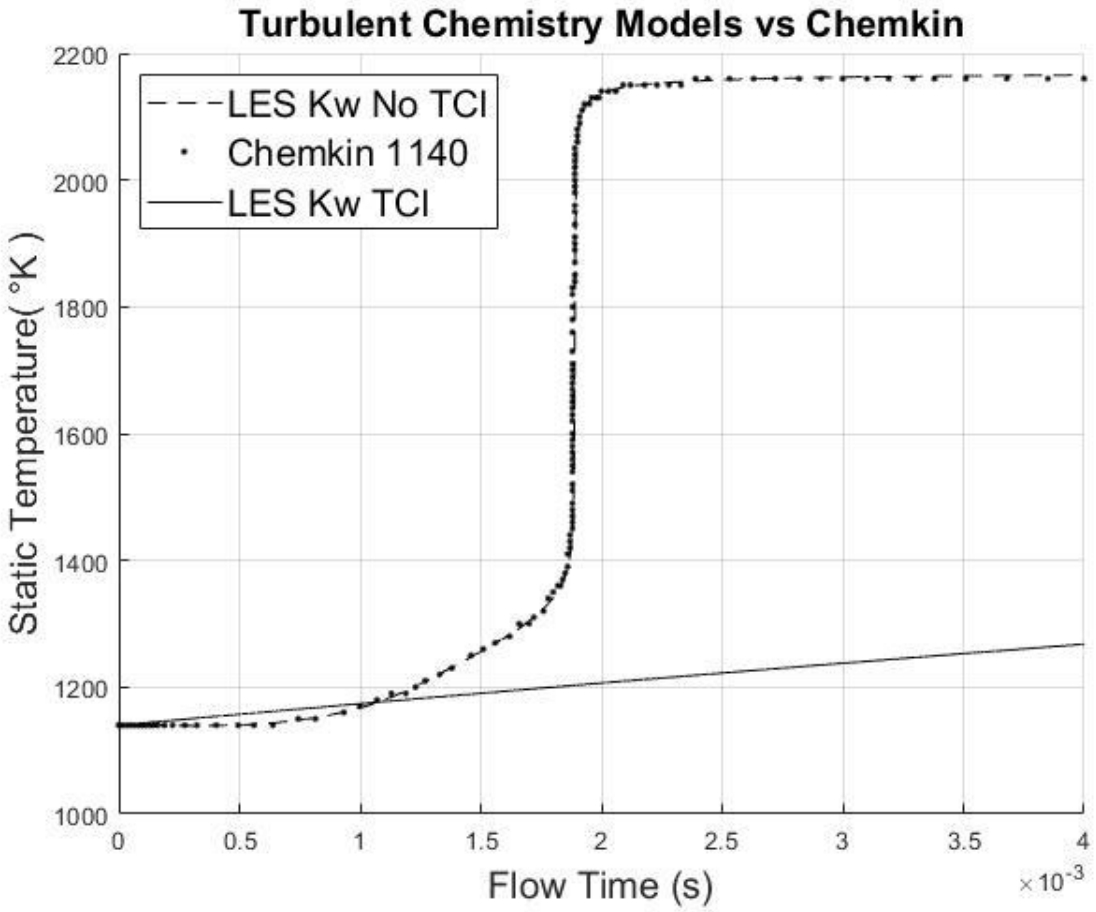

Figure 2: Comparison of Reaction Models against Chemkin Results

Computation expediters were considered for this problem, however, only chemistry agglomeration was found to have a negligible effect on the solution. Chemistry agglomeration compares like cell initial conditions and provides the same solution for comparable cells. An initial bound of 2° K was used however a larger band is likely acceptable and could be used to reduce run time. An *In Situ* Adaptive Tabulation (ISAT) table was tried however the results were found to unacceptably affect the solution.

2.3 Completed Simulation Studies – Time Step and Iteration Independence

For transient solutions through Fluent' s Dual Time-step Integration (DTI) scheme, a balance between time step and iteration must be considered to aid stability and accuracy without unnecessary computation time. DTI is the numeric process of implementing a dummy time which provides stability and accelerated convergence towards the true time step desired [24]. While the velocity time scale relative to the mesh is of consideration for stability, the reaction time scale is much smaller and drives a smaller time step. A preliminary time study was conducted with a KE viscosity model comparing 1 and 0.5 μs which found a negligible difference in pressure through the simulation (less than 2%) however found a spike 14% difference in temperatures during the peak reaction period. See Figure 3. As such the larger time step 1 μs will be used for the bulk of compression before the reaction begins, and 0.5 μs will be used for the reaction and resulting post combustion simulation. While the time sensitivity was done on a different model than was used in the final problem the smallest time scale is the reaction. Number of iterations were also increased for the final solve.

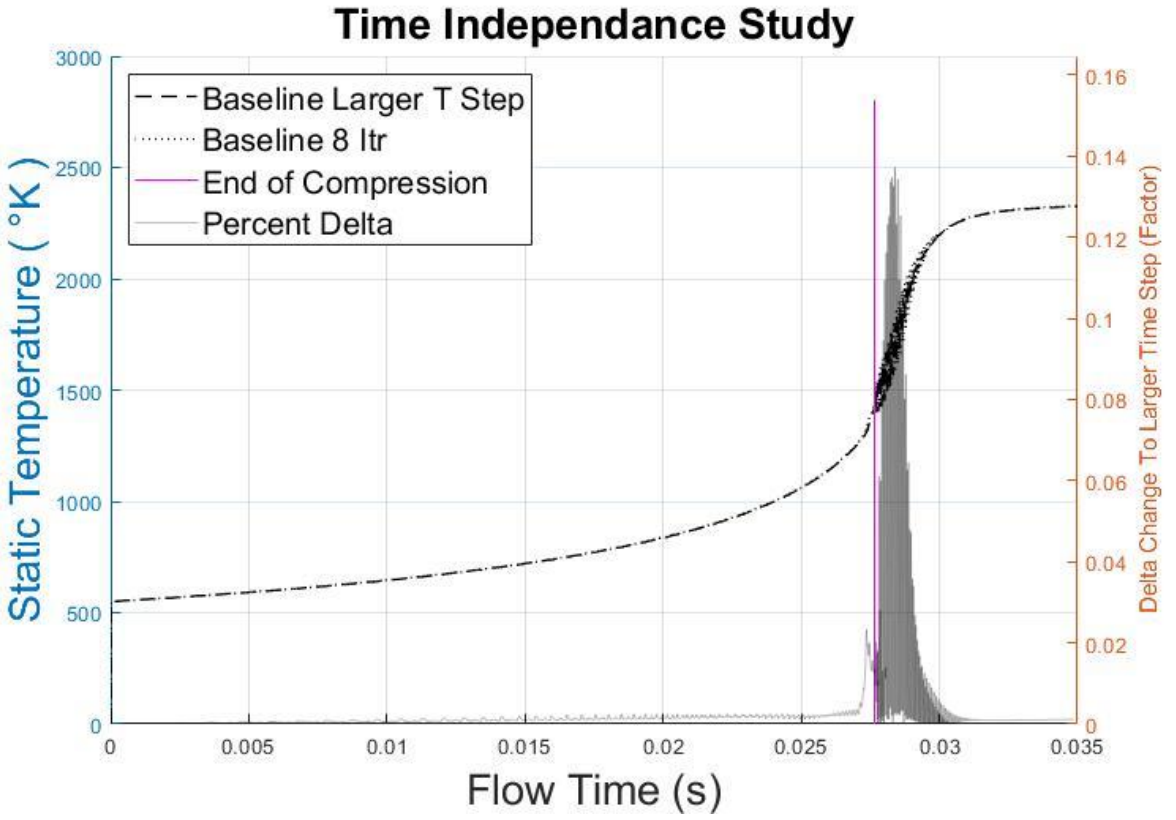
Time Independance Study
Baseline Larger T Step
Baseline 8 Itr
End of Compression
Percent Delta
Static Temperature (°K)
Delta Change To Larger Time Step (Factor)
Flow Time (s)
0
500
1000
1500
2000
2500
3000
0.02
0.04
0.06
0.08
0.1
0.12
0.14
0.16
0.005
0.01
0.015
0.02
0.025
0.03
0.035

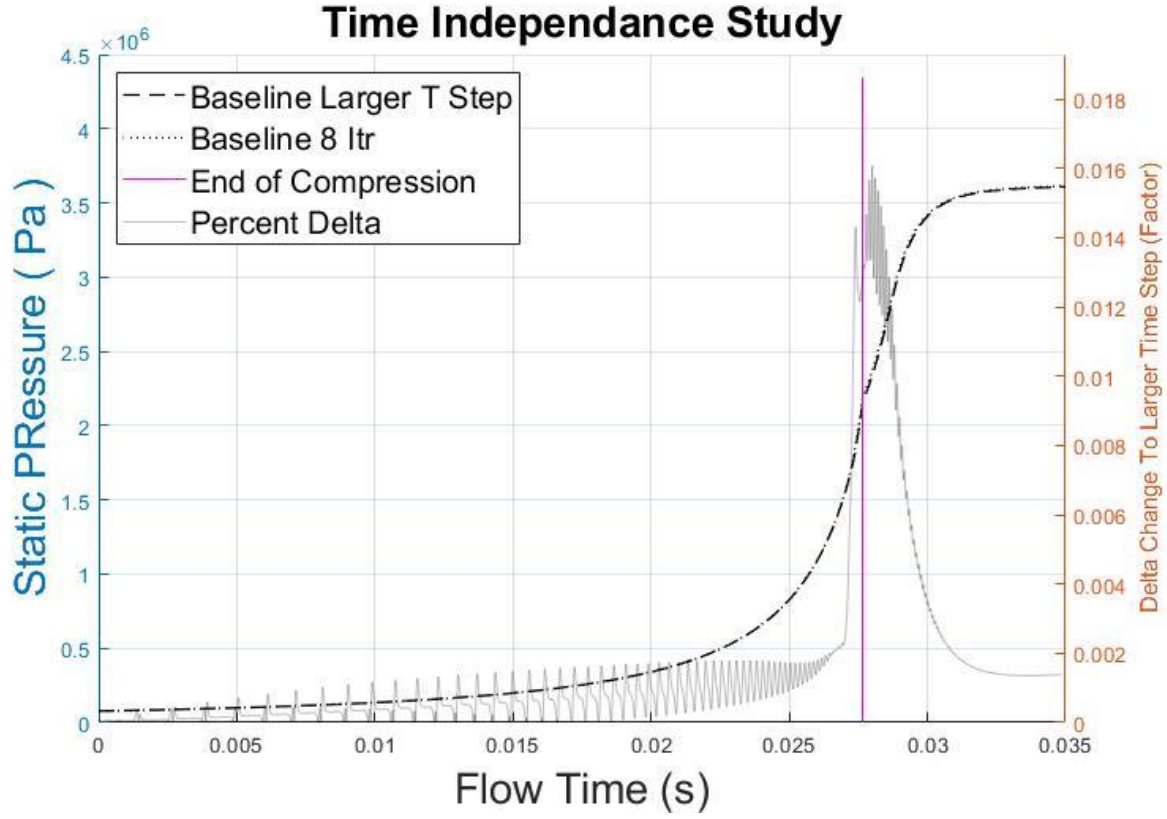
Time Independance Study
×10^6
Baseline Larger T Step
Baseline 8 Itr
End of Compression
Percent Delta
Static PRessure (Pa)
Delta Change To Larger Time Step (Factor)
Flow Time (s)
0
0.5
1
1.5
2
2.5
3
3.5
4
4.5
0.002
0.004
0.006
0.008
0.01
0.012
0.014
0.016
0.018
0.005
0.01
0.015
0.02
0.025
0.03
0.035

Figure 3: Temperature and Pressure Time Study. Percent Delta in black Reported

2.4 Grid Independence and Dynamic Mesh Motion Study

To simulate the single step compression, a dynamic mesh motion scheme was used to reprogram the nodes axially. The scheme is driven by a User-Defined Function (UDF) that saves the initial mesh coordinates and reprograms the axial position of each node at each time step. To control the desired compression ratio, a time cutoff was included in the UDF to stop motion and hold a constant volume past a determined time. Due to single directional remeshing, this scheme warps the aspect ratio of the cell equally with compression ratio. To avoid warping non-Cartesian cells generated around sharp geometry, associated with the variable piston heads, a section of the mesh is not compressed and only translates axially shown in Figure 4. Lastly, to ensure no steep grid gradients at TDC, the non-compressible mesh zone sizing was reduced by a factor of 10. This yields a maximum gradient at the beginning of the problem but is resolved by the beginning of combustion. An additional benefit of a static region methodology is the main interest of the problem is around the variable piston and providing a static mesh reduces numerical error added by a dynamic mesh.

Alternately, a dynamic mesh scheme compressing the region around the piston could have been utilized had the dynamic mesher been leveraged in Fluent. By compressing the mesh around the piston head the mesh would have become finer throughout the solve increasing fidelity in the region of interest. Ultimately implementing an incompressible region prevented altering the non-cartesian mesh with the tradeoff of increasing cells; future studies utilizing the dynamic mesh in fluent could reduce overall mesh count.

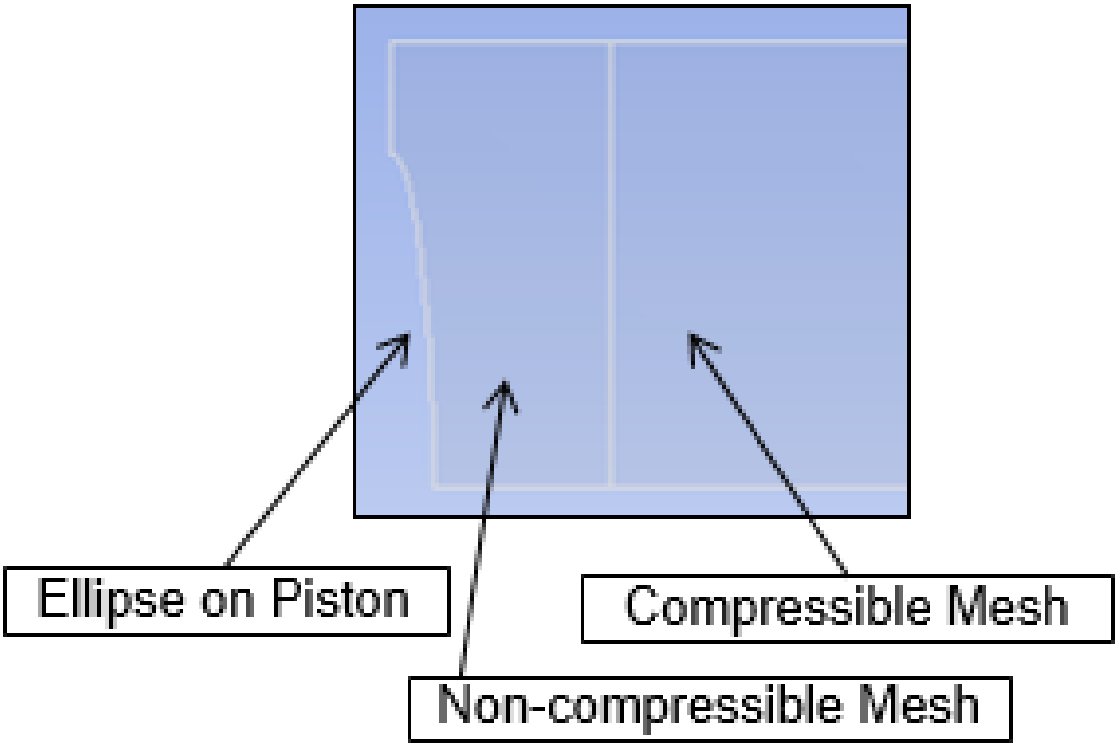

Figure 4: Ellipse Geometry with Static-Mesh Regions Identified

Due to heat transfer across the wall and the no slip condition, the wall mesh was refined locally. To capture such effects, 6 inflation layers on all walls were utilized with a max thickness of 0.001". Using a cell length control of 0.10" globally and 0.01" for the non-compressing region; the baseline mesh case has 156,000 cells. To determine grid independence a refined grid of the baseline case has been kicked off to capture the differences with a finer mesh. Results indicate an overall peak difference of 5.1% at the post ignition.

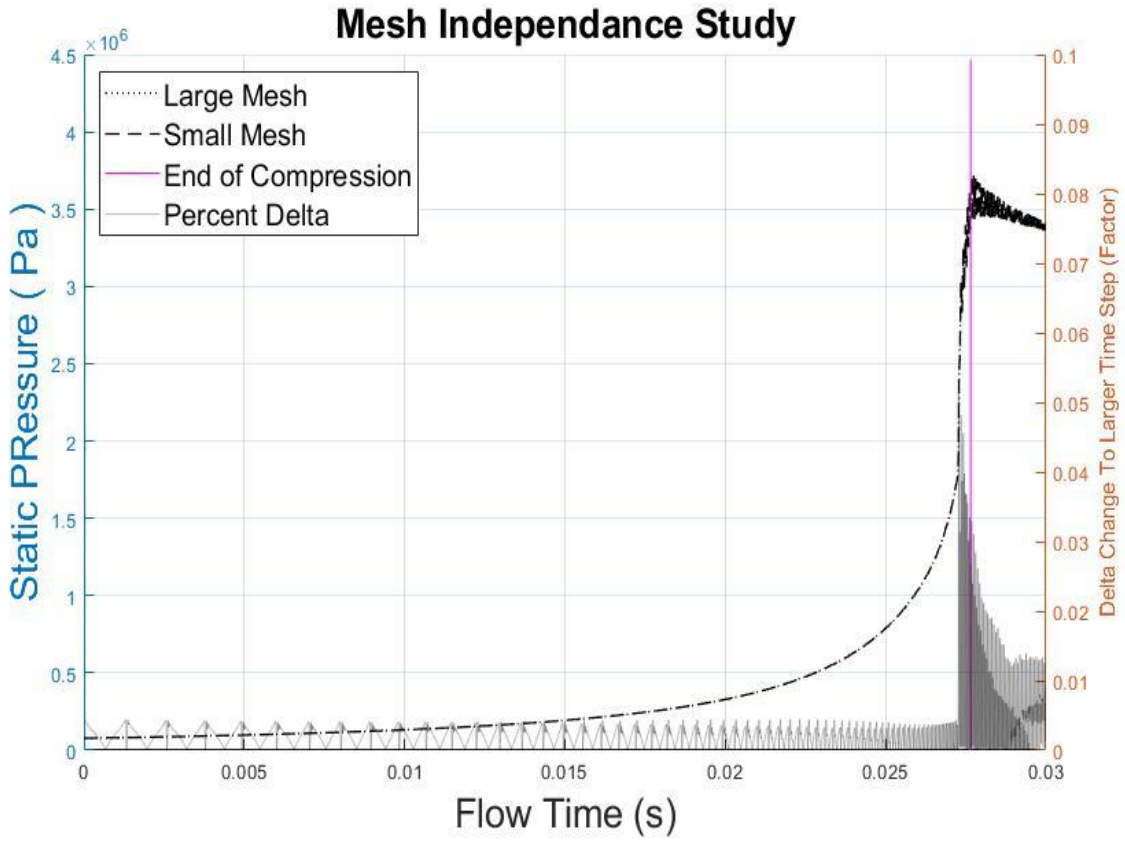

Figure 5: Pressure Monitor Comparing the Baseline Mesh with a Further Refined Mesh

An interesting consequence of the simulated compression step is an acoustic wave that is generated at the start of compression and continues to clearly reverberate through the compression step and into combustion. The acoustic wave is most notable in the velocity monitor output however is seen in other monitors. To study the effect, a ramped UDF profile was utilized to slowly begin compression and bring the piston to speed within 1 ms. This case ended up creating a second acoustic wave; without further insight into which was more engine representative the non-ramped case was selected to reduce the number of waves imposed on the problem. The figure below (right) shows the mass weighted velocity monitor of both the un-ramped (pink) and ramped case (black). The figure on the left shows the calculated peak-peak period of the velocity monitor vs the ideal acoustic period of the fluid considering bulk

temperature and point in time axial length assuming idealized acoustic reverberation and homogenous speed of sound.

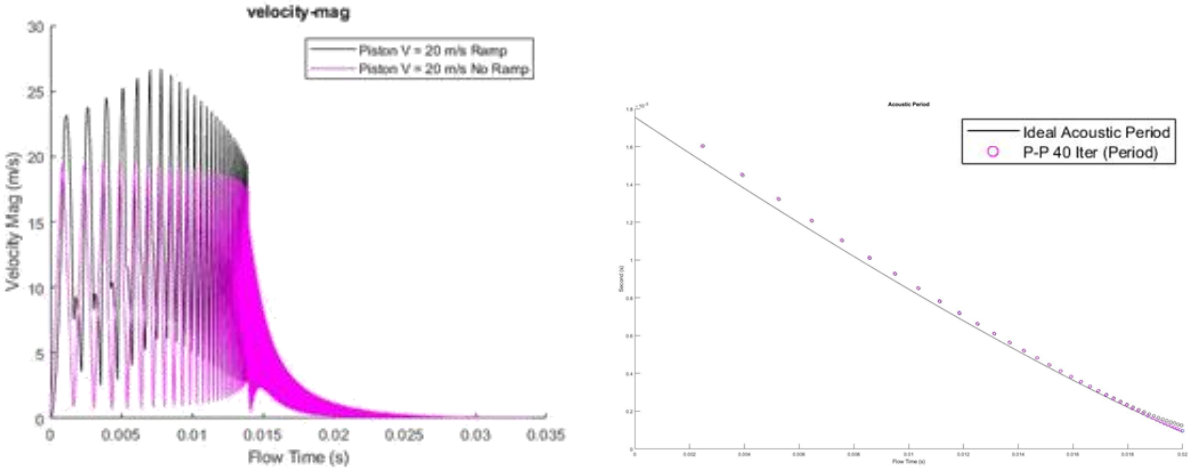

Figure 6: Velocity Monitor vs Time (Left). Ideal Acoustic Time Period and Velocity P-P Period (Right)

Overall piston motion is an obvious variable in real RCM application, early requirements for the pistons required a direct stop after compression [1], but acceleration at start and end of compression was much harder to control. It has been presented in other works that the compression is more gradual both at the start and end in real RCM applications [25]. These effect have not been studies and assumed out by implementing only smooth piston motion and step function start and stop in the UDF program. Future work to study the effects of piston profiles would be interesting.

Chapter 3: Test Matrix

This work sets out to probe the cold roll up vortex generated in a Rapid Compression Machine during compression, alter the structure, and see its effect on the resulting chemical kinetics. This work hopes to identify a reasonable computational model to capture such flow effects and integrate a detailed chemical model to measure the ignition time. Previous work, discussed above, has identified a proposed viscosity and reaction model which aligns with zero-dimensional solvers to ensure complex kinetics accurately resolved. This methodology will be applied to various compression simulations with different piston head geometries in stoichiometric cases of n-heptane.

3.1 Simulation Definition

All proposed simulations will be completed in ANSYS Fluent Version 19R1 and will be 2D transient axisymmetric models. Gravity will be considered counter to piston motion. All simulations will be executed with a hybrid LES/RANS K-ω Shear Stress Transport (SST)-SBES-WALE viscosity model, volumetric finite rate No-TCI reaction model considering stiff direct numeric integration, as discussed above. For computational efficiency chemistry agglomeration will be utilized, currently an error of 0.01 and a selector bound of 2° K.

All simulations will be completed with the dynamic mesh scheme discussed above, with an un-ramped and constant 10 m/s through compression however the time boolean to cease compression will be different to maintain a constant ultimate compression ratio of 10.868. This will yield slightly different compression durations, largest temporal variance is less than 0.3%. All simulations will use a duel time step scheme as discussed above, leveraging large time steps

(1 x 10^{-6} s) though compression and reducing the time step (to 5 x 10^{-7} s) prior to the start of combustion. As discussed this will reduce computational load while attempting to resolve the shorter combustion time scales as needed. In an attempt to refine the acoustic wave generated by the start of compression and promote stability, the complex cases will be started with a set of 50 time steps $5x10^{-7}$ s, compared to the baseline's first 25 time steps of $1x10^{-6}$ s, both solving 100 iterations. This was implemented to resolve the initial acoustic wave generation from the added complex geometry. The remainder of the solution will be executed 40 / 60 iterations pre and post time step reduction respectively. The large iterations is conservative, however through combustion in previous work acceptable convergence was achieved with ~50 iterations and slightly longer solve time was acceptable to increase stability. The problem will be wall bounded by a dynamic piston, a top and axial wall. Wall boundary conditions for all simulations will be no slip, assumed to be a constant 500° K, and a standard roughness of 0.5.

Initial conditions can have a large impact on RCM experiments [6], and absolute control leading to valid concerns about the applicability of fully premixed quiescent flow. However, no further definition and the impacts being outside the scope of this work justify this hefty idealist assumption.

The above considerations will be included however will not be varied across the project. Simulations will be monitored through mass weighted temperature, pressure, velocity, each species in the model will be reported, and contour plots of temperature, oxygen and water will be displayed at intervals of 250 time steps. The thermal contours will be taken with a relative scale from Min-Max temperature in Kelvin to capture the thermal gradients which will be used as a

proxy for flow structure. All simulations will be conducted on Pratt and Whitney's High Performance Computer.

3.2 Variables to Be Studied

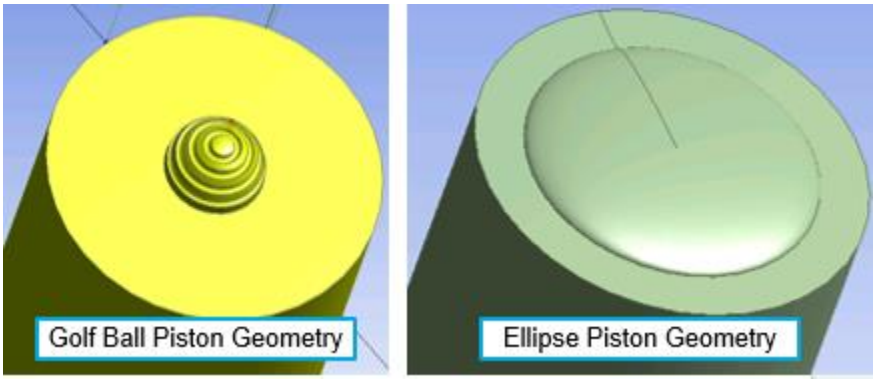

Figure 7: Variable Piston Geometry Studied, Golf Ball (Left) and Ellipse (Right)

The goal of this project is to gain understanding of how the different piston geometries affect ignition delay. The ellipse geometry was chosen since it would provide a large protrusion on the piston. The golf ball was chosen for the sharp cut outs of the sphere and was believed to promote turbulence. Both of these geometries were sized conservatively small for stability to require a small static region. The proposed work is outlined below in Table 1.

Table 1: Proposed Matrix of Simmulations; Color Coated with Corresponding Phase

Runs Description					Initial Condition	
Priority	Piston Geometry	Fuel (Chemical Model)	Equivalence Ratio	Wall BC	Temp (°K)	Pres (kPa)
1	Baseline	Reitz 29 Species nHept	Stoicheometry	500 K	550	77.0
1	Ellipse		Stoicheometry	500 K	550	77.0
1	Golf Ball		Stoicheometry	500 K	550	77.0

Chapter 4: Results

4.1 Flow Structure through Compression

A qualitative assessment of the thermal contours demonstrates the formation of the cold roll up vortex and shows the flow structures generated are highly impacted by the variable piston geometry. Thermal contours are used heavily in combustion to study flame structures and can be used to characterize aerodynamic structures. The cold roll up vortex is easy to track through thermal contours due to the inherent temperature gradient between the cold air from the boundary layer and the far field gas. The contours have been concatenated for a video in time. It appears as if the piston slows down at the end of compression; this is due to an increased frequency of output contours and a uniform concatenation time.

Figure 8: Baseline case through compression, CR = 1.44

Figure 9: Baseline case through compression, CR = 2.98

The baseline case shows a vivid cold roll up vortex generated through compression. This finding is aligned with previous characterizations [10]. As the piston compresses the air domain it shears along the axial cold boundary creating a cold gas swirl (the cold roll up vortex). Aligned with expectations the vortex is generated at corner between the piston and axial wall, seen in Figure 8. The vortex then grows in size and travels radially inwards towards the RCM centerline, shown in Figure 9. As the vortex travels inwards it partitions the warm air. As the vortex grows, the tail begins to shed into the wake of the main vortex and the recirculation beings to grow on the outside of the vortex. The wake pushes the vortex and causes the roll up to fold over enveloping a warm pocket of air, show in Figure 10.

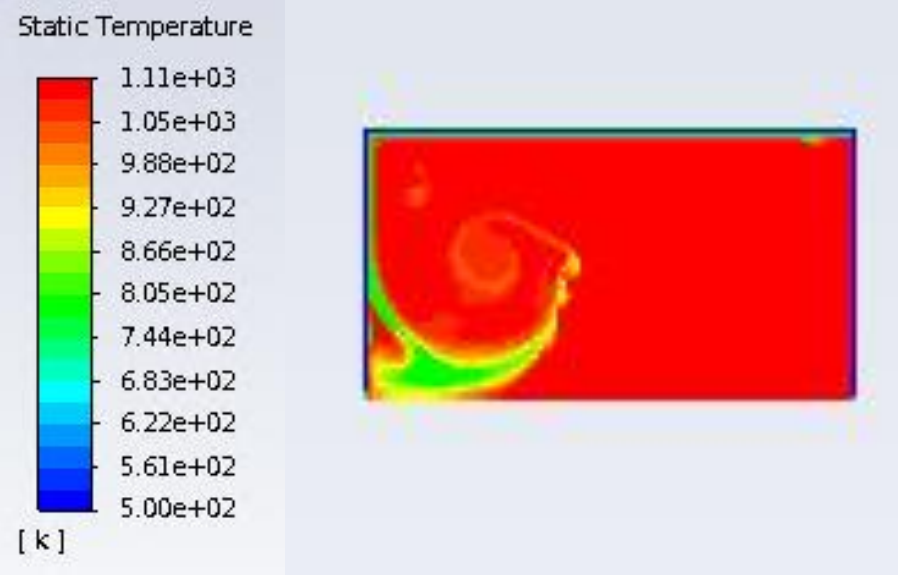

Figure 10: Baseline case through compression, CR = 6.12

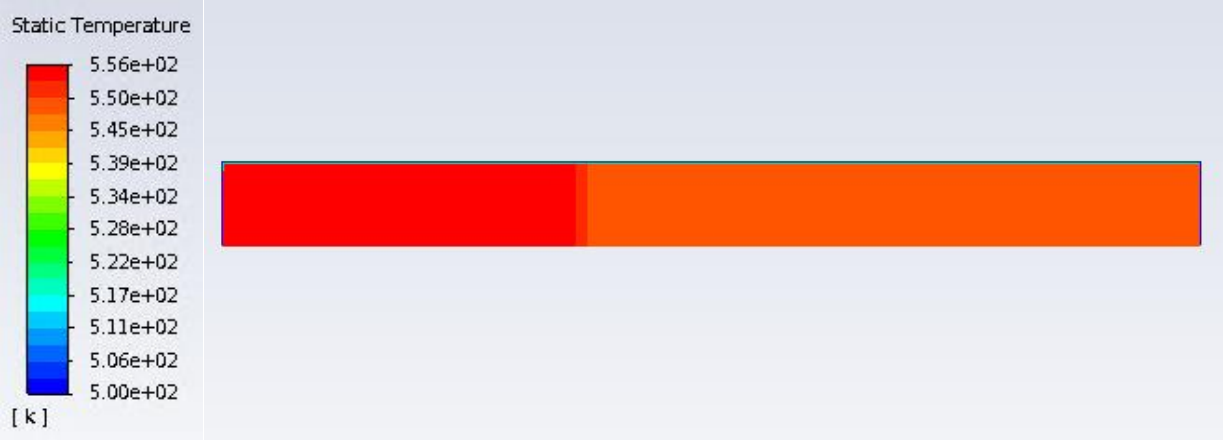

Figure 11: Baseline Case, Time = 0.125 ms

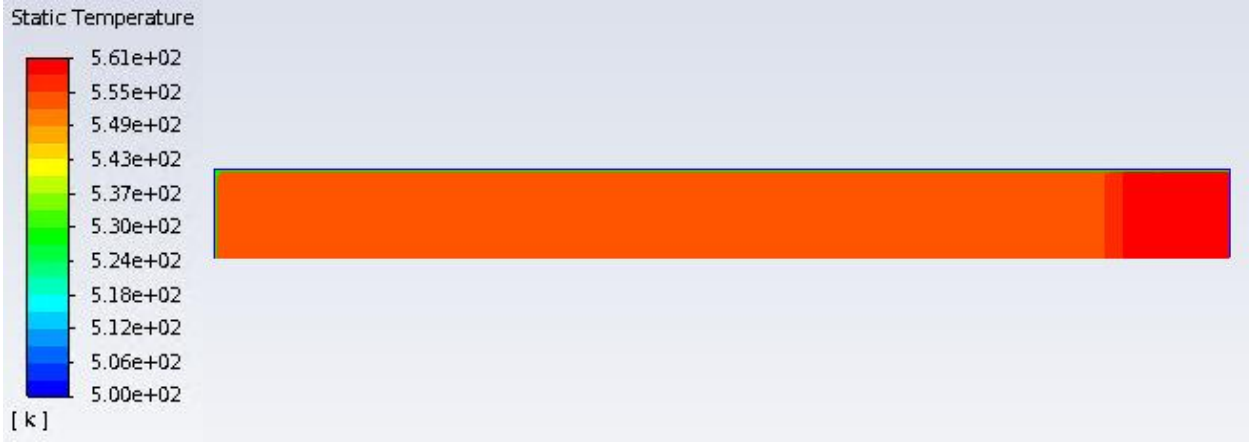

Figure 12: Baseline Case, Time = 0.375 ms

Discussed above, an acoustic wave generated from the initial piston motion is observed reverberating in the air domain through compression. Figure 11 shows the first thermal contour taken at time 0.125 ms. A clear compression wave divides the air domain between into two temperature regions. The wave is seen traveling down to the top wall (right end of the air domain) before reverberating and traveling backwards towards the piston. Figure 12, taken at time 0.375 ms, shows the wave after reverberating on the top wall where the high thermal region is now between the wave and the top wall.

Figure 13: Golf Ball case through compression, CR = 1.43

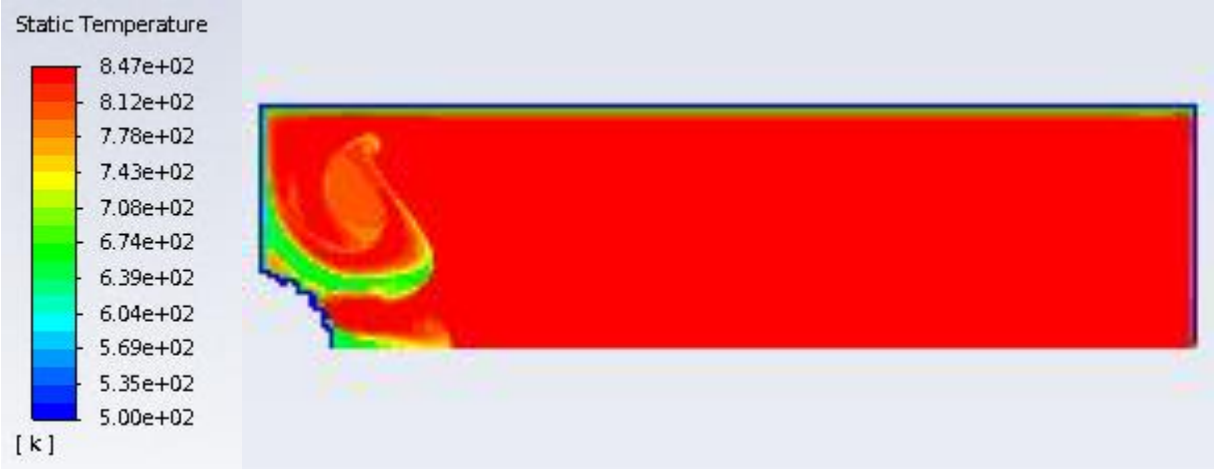

Figure 14 : Golf Ball case through compression, CR = 2.97

The flow structures initially generated in the golf ball case are similar to the baseline case, however additional vortices were generated from the dimple cut outs of the golf ball. Comparing the golf ball and baseline case, an almost identical main roll up vortex from the piston / axial wall corner is formed early in compression. This makes sense as the geometries are very similar at the Outer Diameter (OD) portion of the piston. A similar cold roll up phenomenon occurs in the circular dimple cut outs. Two smaller vortices are of interest, shown in Figure 13, one that generates at the radial OD of the golf ball and the other at the Inner Diameter (ID) centerline. The OD roll up is enveloped by the main vortex upon interaction leading to a small warm pocket, seen in Figure 14. The interaction between the main roll up and the ID vortex is more complicated. As the main vortex travels to the centerline and begins to near the ID vortex the main vortex is forced backwards (radially OD). As the main vortex it forced outward it sheds an eddy. This spin off leads to a sharp cold gas region that wraps around the protrusion, and a new cold gas flow structure in the middle of the domain.

Figure 15 : Ellipse case through compression, CR = 2.99

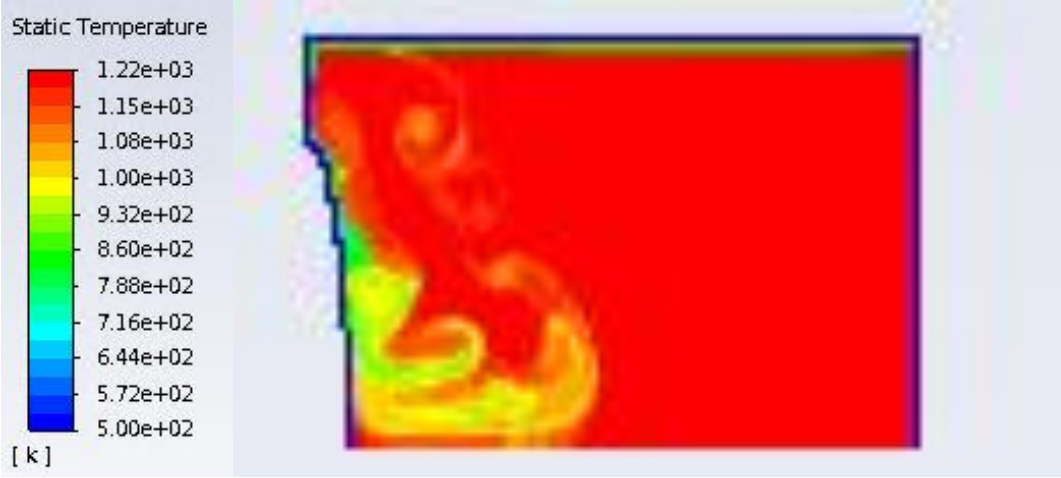

Figure 16: Ellipse case through compression, CR = 7.80

The ellipse case shows the most breakup of the main roll up vortex smearing the cold gas region proving the most well mixed contour at TDC. Similar to the baseline and golf ball cases, an initial cold roll up is generated from the piston-axial wall corner. This case is different as the protrusion geometry takes up more radial length so the main vortex interacts with the piston geometry earlier in time. As the main roll up vortex travels towards the center line, it washes over the ellipse geometry and sheds an eddy, seen in Figure 15. The detached eddy is observed to

travel through the domain and impinge on the axial wall before dissipating. By Compression Ratio ~7.8, seen in Figure 16, the main vortex has folded over onto itself and is very broken up. In the break up many smaller eddies are seen on the perimeter, and warm pockets of air are mixed with the cold roll up core. Ultimately this leads to a much smeared cold gas region with the most well mixed thermal contour prior to ignition.

4.2 Thermal Monitor through Compression

The temperature monitor throughout compression shows a steady and intuitive gain with decreasing rise as Compression Ratio (CR) increases.

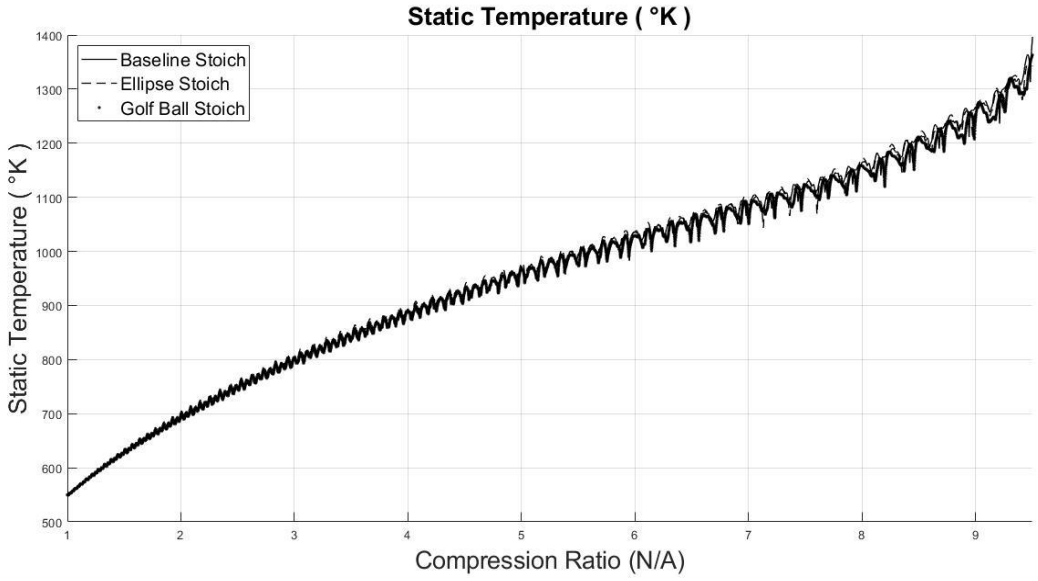

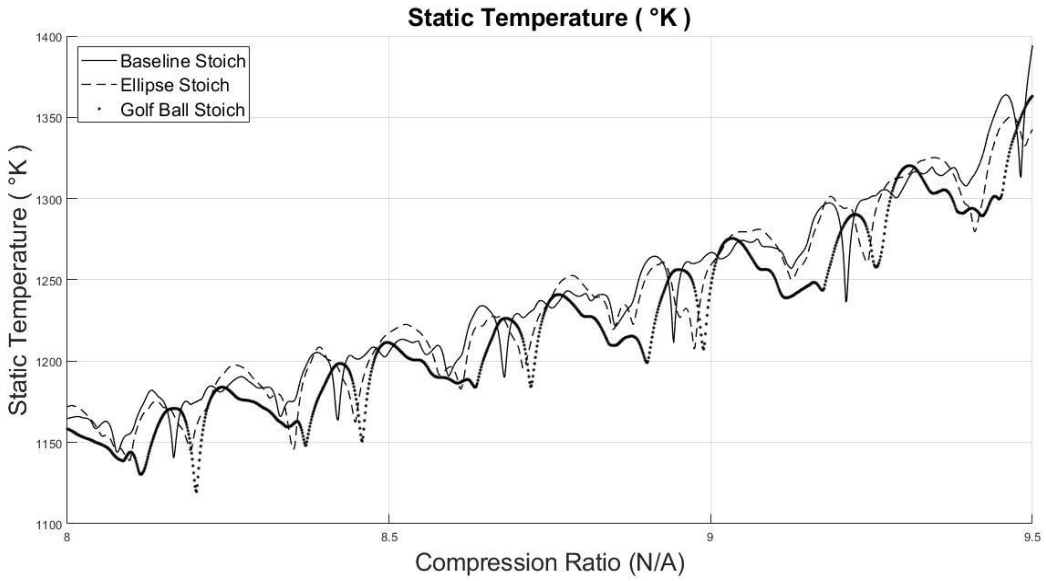

Figure 17: Temperature vs Compression Ratio Whole Trace (Top) and Zoomed Section (Bottom)

Two causes for the decreasing temperature gain is increased heat lost through the boundary and the decreasing work done on the system from marginal volume reduction. As the gas is compressed, kinetic energy increases within the fluid shrinking the boundary layer around the domain of the problem. This increases convective heat transfer and increases energy lose to the cold wall and the ambient. The tapering off of temperature gain relative to compression ratio can be explained by assuming isentropic compression for most of the domain. As the compression ratio increases, as the marginal volume reduction leads to a lower temperature rise as temperature increase is the inverse CR is taken to the gamma - 1 power.

4.3 Flow Structures before Ignition

Direct comparisons across all three cases is difficult due to the constant piston velocity and contour capture rate but variable compression rates in time. As such a contour directly preceeding the main ignition and directly following will be assessed.

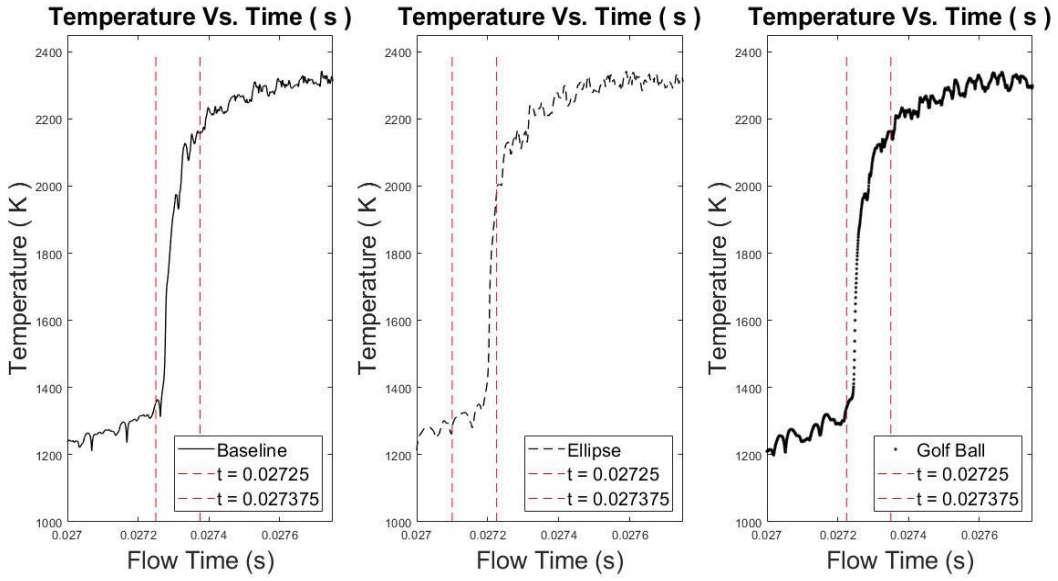

Figure 18: Contour Capture Relative to Temperature in the Baseline (Left), Ellipse (Middle), and Golf Ball (Right) Cases

Figure 18 shows when the pre and post ignition contours were captured in bracketed red lines, vs the solution temperature monitor vs time. The differences in contour capture times are due to the offset points of ignition relative to time. Keeping the piston velocity a controlled variable was important, which caused a constant reduction in the volume through time. Since the variable geometries caused different initial volumes the relative compression rate in time is slightly different. This is most noticeable for the ellipse case, which had the most volume lost due to the piston, and is thus shifted forward in time. This shift slightly changes the temperatures relative to the contour captures. The baseline and golf ball nicely bracket the ignition, the ellipse case has contours earlier and in the middle of the ignition. The ellipse overall temperatures are

therefore lower at time of capture relative to the baseline or golf ball case. Looking through the contours, the flow structure is unlikely to change drastically in the next fraction of a second and the qualitative observations are believe to be comparable.

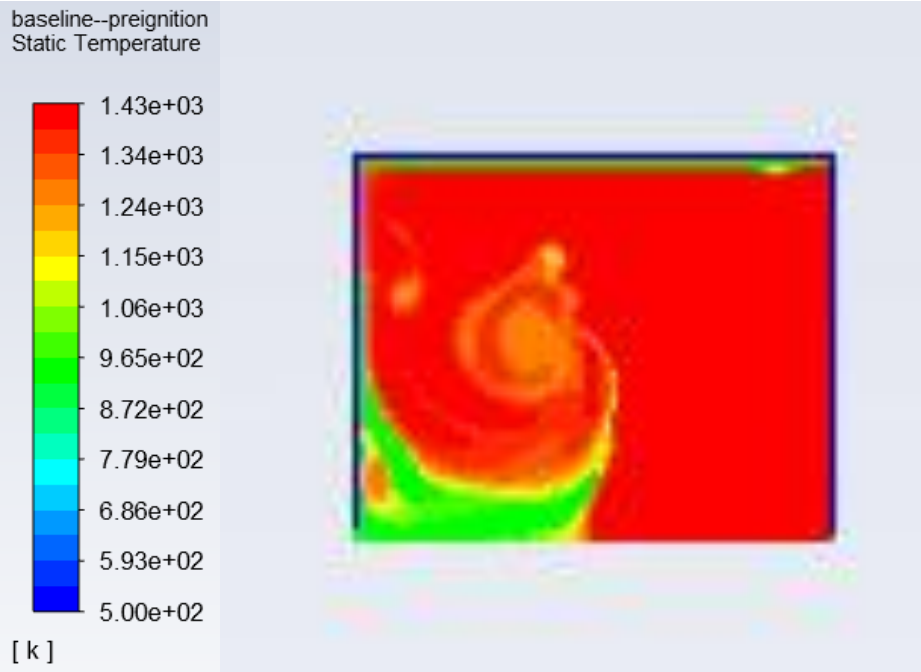

Figure 19: Baseline Case Thermal Contours Directly Proceeding Ignition (°K)

Seen in Figure 19, the baseline geometry case has a sharp cold roll up vortex. A large tip vortex of warmer air is also apparent and smaller eddies are seen in the wake. The baseline case has a warm pocket of air which was enveloped during compression near the heart of the cold gas region.

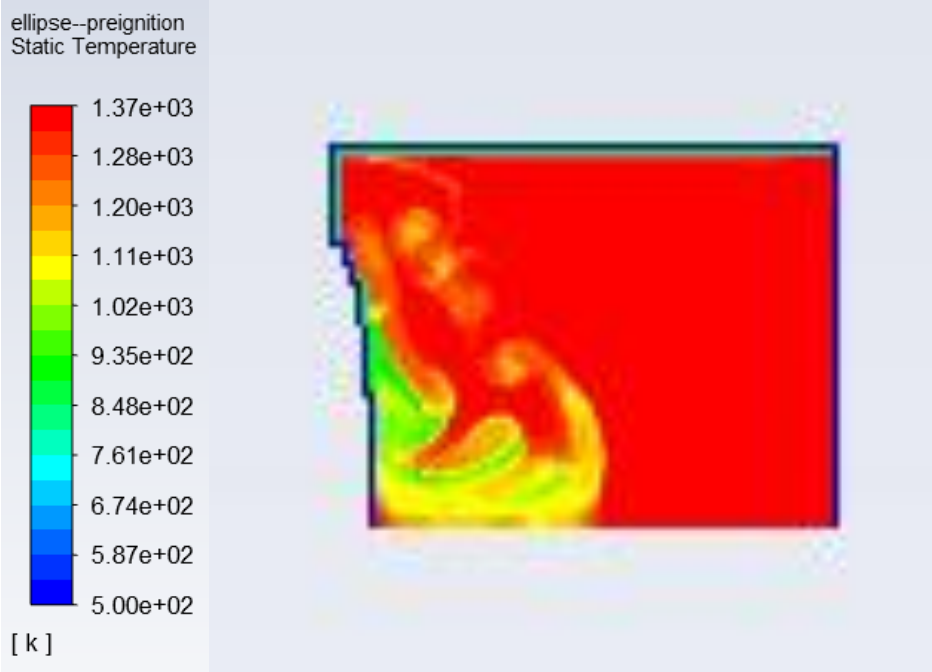

Figure 20: Ellipse Case Thermal Contours Directly Proceeding Ignition (°K)

The ellipse case, shown in Figure 20, shows a more complex broken up cold roll up vortex yielding the most uniform thermal contour across all cases. While, the contour is captured earlier in time, leading to a reduced peak temp, the overall structure is warmer with the least area below 1000° K. The structure is not a coherent recirculation but a series of smaller vortices. These cold vortices are fairly spaced out, taking a good deal of axial length; given the early capture time, it is likely this structure is rapidly compressed.

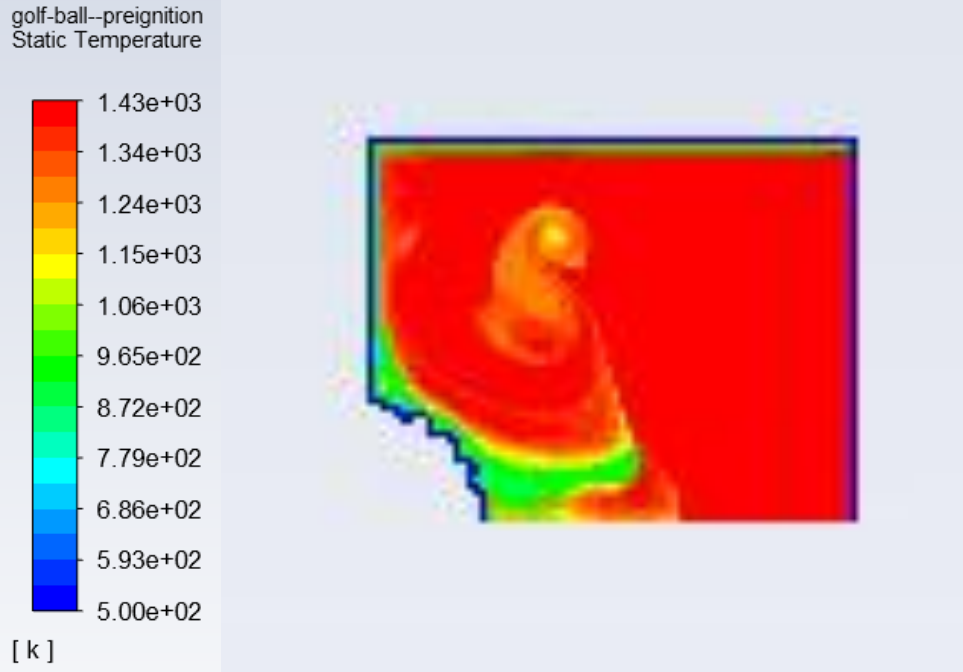

Figure 21: Golf Ball Case Thermal Contours Directly Proceeding Ignition (°K)

The golf ball case, shown in Figure 21, has a similar structure to the baseline case; a fairly intact cold roll up vortex near the centerline, with a shed vortex from the main roll up. The golf ball case is different than the baseline case as the cold region is smaller, and there is no fully enveloped warm pocket of air. Due to a strong recirculation in the baseline case, the tip swirls in the wake of the main vortex. Due to the multiple vortex interaction during compression, the golf ball case appears to shed the tip of the main roll up, this smaller eddy travels radially outwards outward of the wake. It is interesting that almost all the vortices we able to meld together and form a coherent structure with few warm pockets. The ID roll up, although small, near the centerline remains apart from the main vortex.

4.4 Ignition Timing

This investigation assessed the reaction monitor vs flow time and compression ratio, finding an almost negligible different in the bulk reaction time. Bulk reaction times were found to be within less than 4% of each other. The initial condition chosen for this study was high leading to ignition prior to TDC. While this is generally chosen in engine design to achieve maximal power output from in an Otto Cycle [26], many RCM studies look to reach full compression prior to ignition. This would have added the additional variable of structure dissipation after compression.

This leads to two different comparison to make, one in true time and one in relative compression ratio. These two quantities are going to be different since the problem set up outlined constant piston velocity in time instead of constant compression ratio gain in time. Regardless of the comparison the temperature monitors are in near alignment.

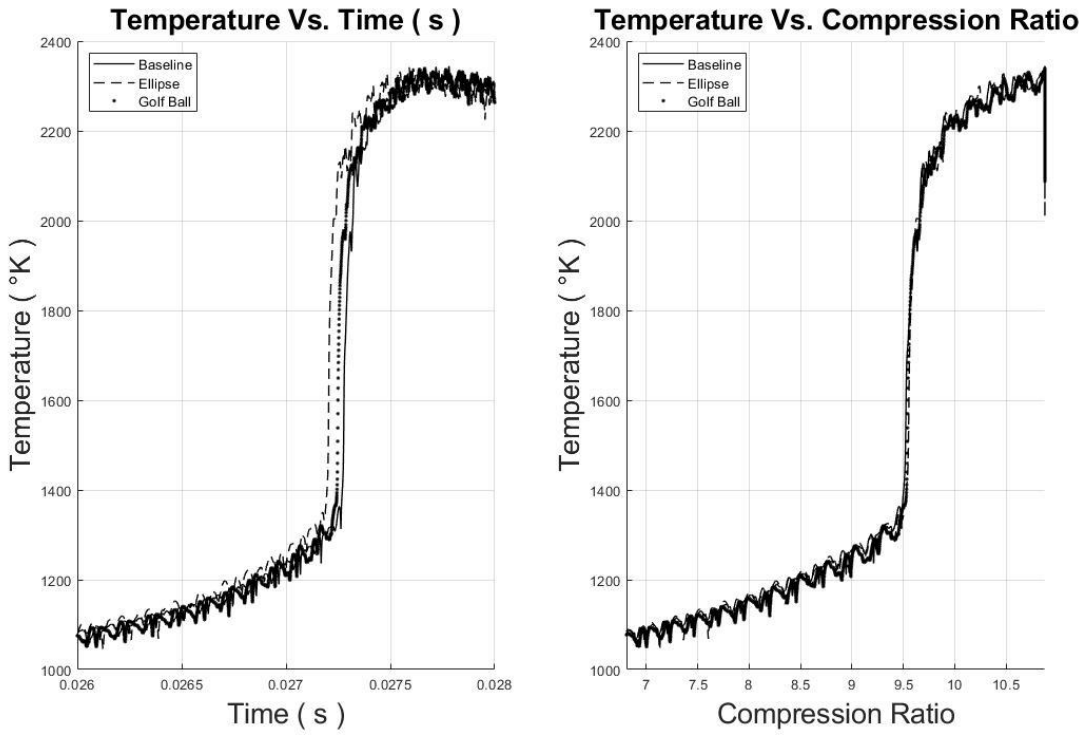

Figure 22: Temperature Monitor vs Time (Left) and Compression Ratio (Right)

The temperature monitors vs compression ratio shows the baseline case reacts first compared to the golf ball and ellipse. Starting from a comparable point at a ratio of 9.4 and temperatures of 1300° K the baseline sees an increase of 400° before the other cases, one metric for assessing ignition delay. This leads to the claim that the baseline case has the lowest ignition delay time. Normalizing for compression ratio is a good comparison as isentropic compression is tied to reduction in volume. Assessing total combustion time is trickier as the cases aggregate after an initial ignition and as the smaller flow structures combust.

While normalizing for compression ratio allows an ignition comparison between the cases relative to the points of in compression, the reaction is a temporal phenomenon not directly tied to compression ratio. This is important as the non-uniform compression rates stretch the

temporal phenomena due to the accelerated volume reduction due to the piston protrusion; the ellipse has most volume loss (-0.32%) vs Golf Ball (-0.16%) relative to the baseline case at top dead center. So, comparing the non-normalized temperature monitors vs flow time allows for a secondary comparison of reaction timing. Versus time, the trends are almost flipped, and certainly stratified in an expected way due to the volume reduction. Looking at the raw temperature plots it was postulated that the ellipse has the steepest temperature gain. This was assessed by calculating a numeric first order derivative in time, shown below in Figure 23.

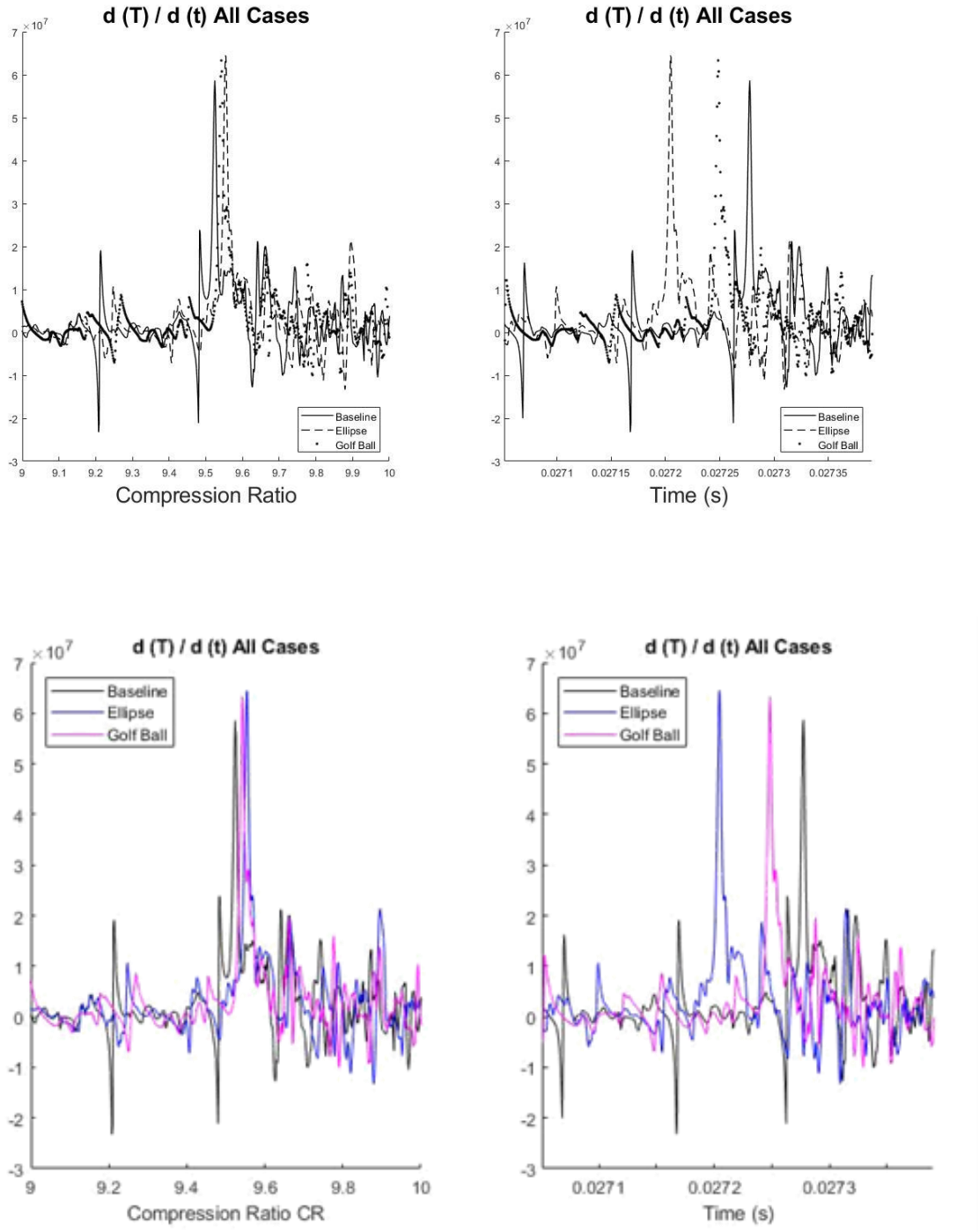

Figure 23: Temperature Derivative vs Time (Right) and Compression Ratio (Left)

Looking at the derivative the ellipse case has the highest nominal gain, indicating the most efficient and largest heat release occurring at some time in the combustion process. It is

important to note that the main goal of the studying ignition delay is to understand the reaction kinematics prior to the main heat release and understanding the mechanisms that lead to auto-ignition. The most uniform heat release, as will be explained below, is attributed to the dispersed vortex roll up which is a topic of this work.

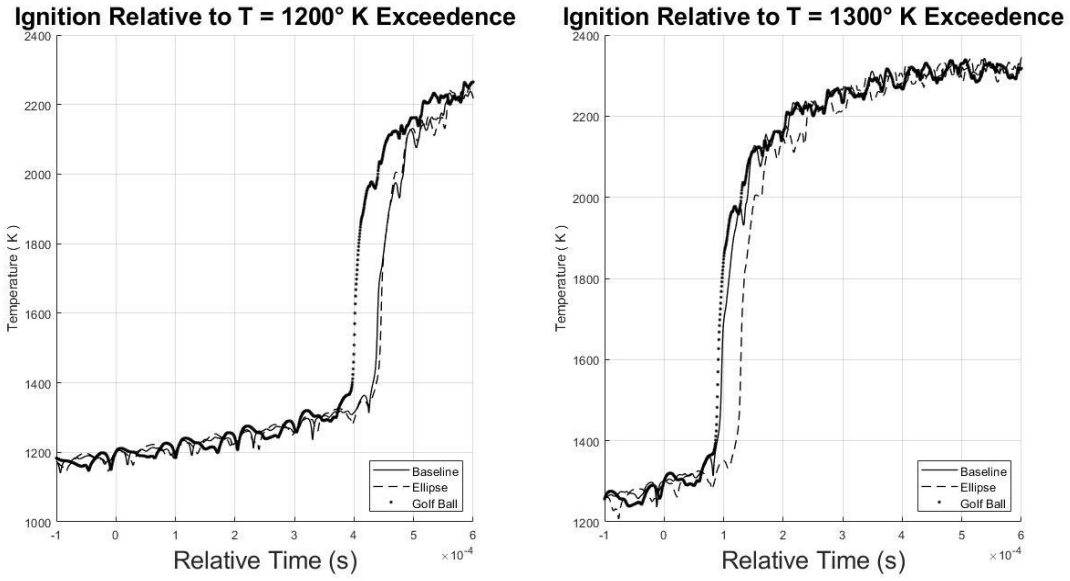

Figure 24: Temperature vs Time Adjusted for First exceedance of 1200° K (Left) and 1300° K (Right)

Other comparisons were used to analyze the data however can be prone to manipulation, so are not reliable comparisons. An example is comparing relative time to a common landmark. Due to numeric fluctuations normalizing the raw temperature signal to the first exceedance of 1300 K can falsely align ignitions in relative time. Seen above in Figure 24, there is pretty good alignment between the golf ball and baseline case if 1300° K is chosen as the landmark. The two cases see an ignition roughly 0.1 ms after this landmark whereas the ellipse case takes about 0.125 ms (a 25% increase in time) before igniting. The temperature monitor, as an enthalpic property, was mass weighted to will provide a bulk measurement which smears the max, min and skewness but is still prone to numeric fluctuation. The flaw in this comparison is seen when

1200° K is chosen and the baseline and ellipse align. A possible counter point is that different temperatures could drive different chemical pathways, this will be assessed after, however there is not meaningful interpretation for ignition delay timing if prone to manipulation.

One interesting aspect is the similar shapes of the reaction curves. Both the golf ball and baseline case see a temperature dip after the first ignition. This aligned feature which is identifiable in the Figure 24 right plot, justified by first 1300° K exceedance, indicates similar post ignition phonemic related to the flow structure.

Table 2 : Reaction Times for Each Case

Case	5% of Peak C7H15-2 Reaction Start (ms)	T Ultimate Pressure Reaction End (ms)	Reaction Time (ms)	Delta To Baseline
Baseline	24.57	27.78	3.208	--
Ellipse	24.50	27.59	3.094	-3.6%
Golf Ball	24.54	27.66	3.127	-2.5%

Ignition delay assess the time required for fuel to work through chain branching, and release enough heat to force a global ignition and sustain a fire. A common measurement of ignition delay is the time between TDC and ultimate pressure. Hence, ignition delay is hard to fully characterize in problems where ignition occurs prior to TDC since the beginning and end are ill defined. Instead this work looked to get a sense of relative reaction timing by determine the interval between an identified beginning and end of reaction. Assessment of the ignition timing found a max 3.6% change between the baseline and complex geometries. The difference between the baseline and ellipse reaction time was 0.114 ms. This is fairly low when compared to the reaction time scale. The beginning of the reaction is characterized by a large presence of

C7H15-2, the first fuel decomposition reaction product. To get over a noise threshold, the time at which mass fraction of C7H15-2 was 5% of the peak was chosen as the start. The end of the reaction was then chosen as the time of ultimate pressure. Ultimate pressure has some flaws, given the baseline and golf ball cases reach ultimate pressure after TDC but the ellipse reaches it before. However other metric such as incremental temperature gain, ultimate temperature, or ultimate product formation yielded similar results. This metric also only looks at bulk characteristics as minor reactions were still occurring after TDC but pressure was falling due to significant heat loss on the system.

4.5 Qualitative Assessment of Burn Structures through Thermal Contours

A qualitative assessment of the reaction finds that the ellipse case has a very even burn, the golf ball and baseline cases have fairly similar stratified burn, but the golf ball's lingering cold vortex regions lead to an extended overall reaction.

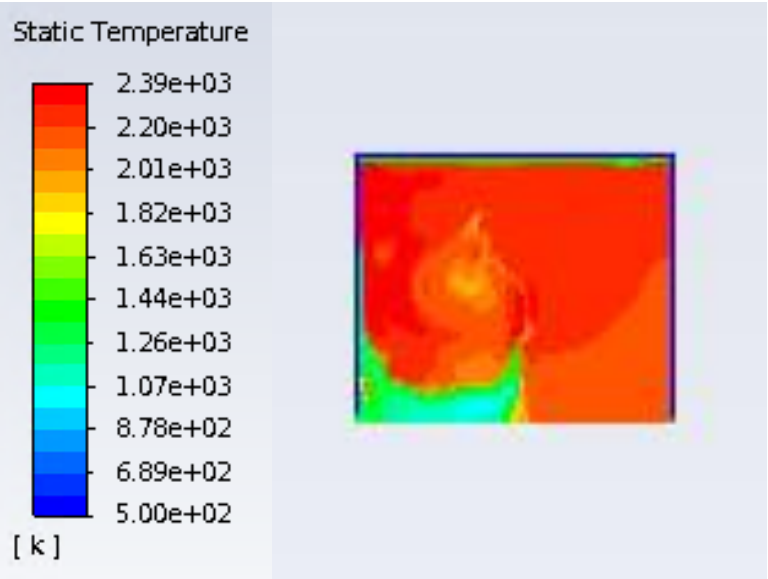

Figure 25: Thermal Contour of Baseline Case after Ignition

The baseline case yields a fairly intuitive burn structure, warm regions react fairly uniformly, and colder pockets of gas generated during compression slowly burn as the perimeter is heated and a reaction is propagated through the fuel. In the first time period of the reaction, reference Figure 18, warm gas outside excluding the boundary layer and cold roll up ignites. The flow bulk flow field goes from roughly 1400° K to 2200° K. This is aligned with theoretical expectations of an RCM which produces near adiabatic compression and uniform reaction. The cold roll up region sees very little temperature gain and thus does not ignite.

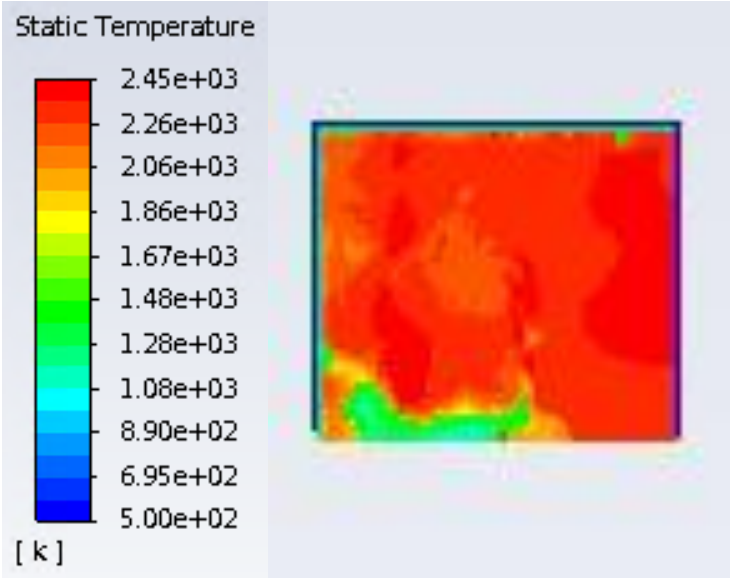
Static Temperature
2.45e+03
2.26e+03
2.06e+03
1.86e+03
1.67e+03
1.48e+03
1.28e+03
1.08e+03
8.90e+02
6.95e+02
5.00e+02
[k]

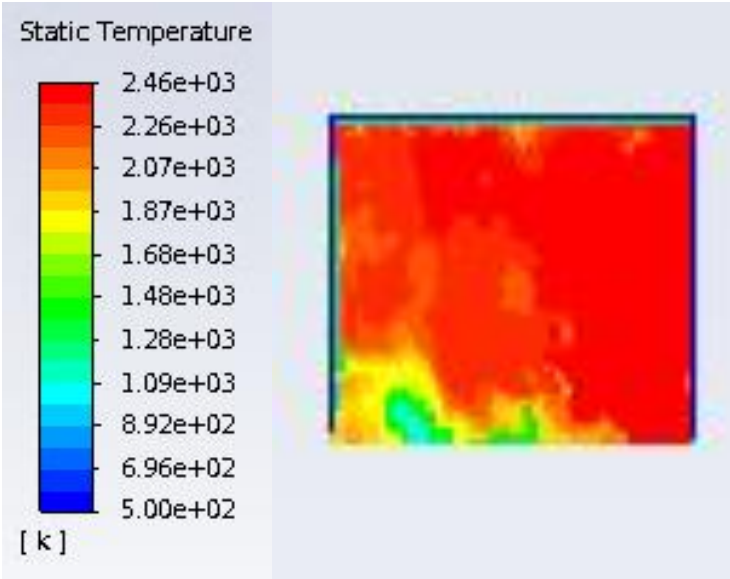
Static Temperature
2.46e+03
2.26e+03
2.07e+03
1.87e+03
1.68e+03
1.48e+03
1.28e+03
1.09e+03
8.92e+02
6.96e+02
5.00e+02
[k]

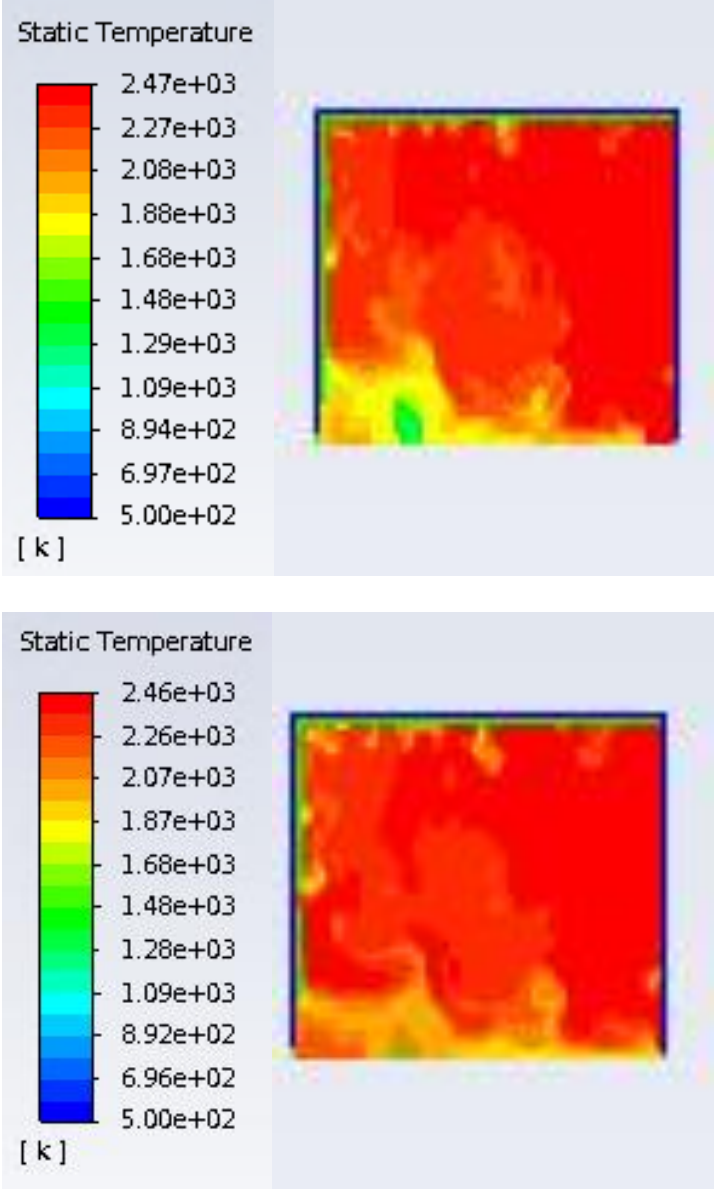

Figure 26: Thermal Contour of Baseline Case through Combustion, Starting t = 27.5 in 0.125 ms Increments

As the cold roll up burns, there is little change to max temperature of the problem but the cold region shrinks. The burn of the cold region is analogous to droplet burning where energy and warm radical diffuse inwards preheating the reactants, but is different as the cold pocket is non spherical. The warm pocket presented in Figure 19 ignites roughly at the same time as the far field flow. This leads to the cold region being completely enveloped by warm products

accelerating the cold gas reaction. This increases the efficiency of the reaction through the end of combustion. The last straggler of cold fuel is observed in the last frame of Figure 26, but is not seen in the frame taken at 28 ms indicating the total burn is bounded by frames representing 0.75 ms.

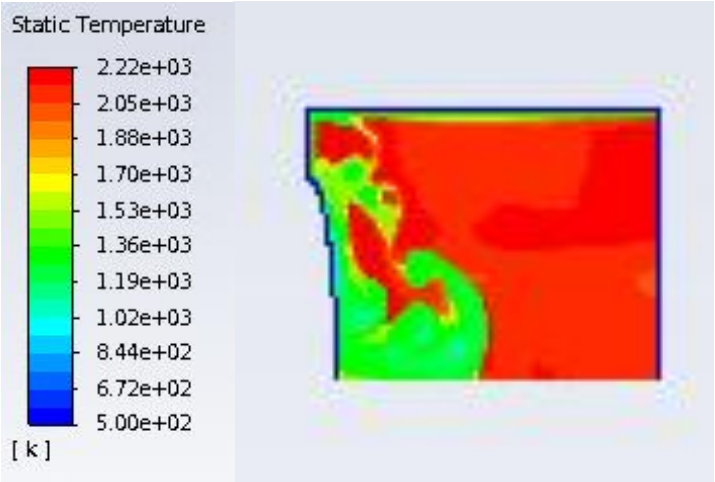

Figure 27: Thermal Contours of Ellipse Case after Ignition

The thermal contours of the ellipse case, Figure 27, shows a stratified burn structure. Due to the cold roll up vortex collapsing over the protrusion on the piston, the field is fairly well mixed prior to ignition. This leads to an even burn in the far field region during the first ignition. The cold gas in the roll up vortex sees a uniform temperature gain while maintaining some stratification. Looking through the rest of the burn, shows slight non-uniformities, however an overall quick reaction.

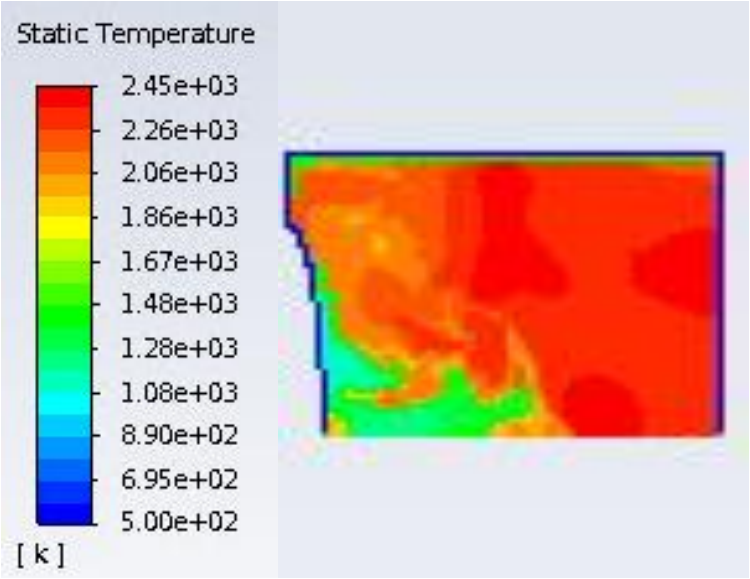
Static Temperature
2.45e+03
2.26e+03
2.06e+03
1.86e+03
1.67e+03
1.48e+03
1.28e+03
1.08e+03
8.90e+02
6.95e+02
5.00e+02
[k]

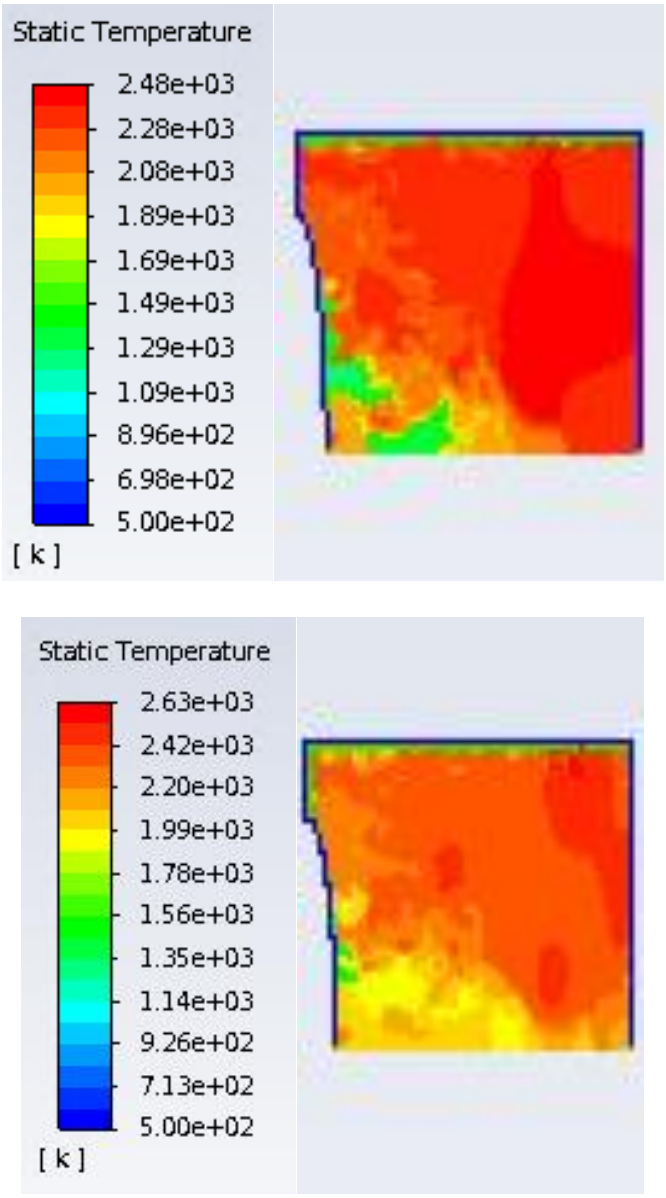

Figure 28: Ellipse Case through Combustion, Starting t = 27.350 ms in 0.125 ms Increments

The first contour post ignition, in Figure 27, looks homogenous in the roll up region. However, successive frames, seen in Figure 28, indicate there is a colder core in the middle of the vortex that burns more slowly. Unlike the baseline case the cold gas is not completely surrounded by warm air so gas near the piston does not burn evenly. A lot of mixing is apparent and the warm product in the far field are cooled as the cold gas dissipates. The overall

assessment of the ellipse case reaction to be bounded within 0.625 ms, which is still lower than the baseline case.

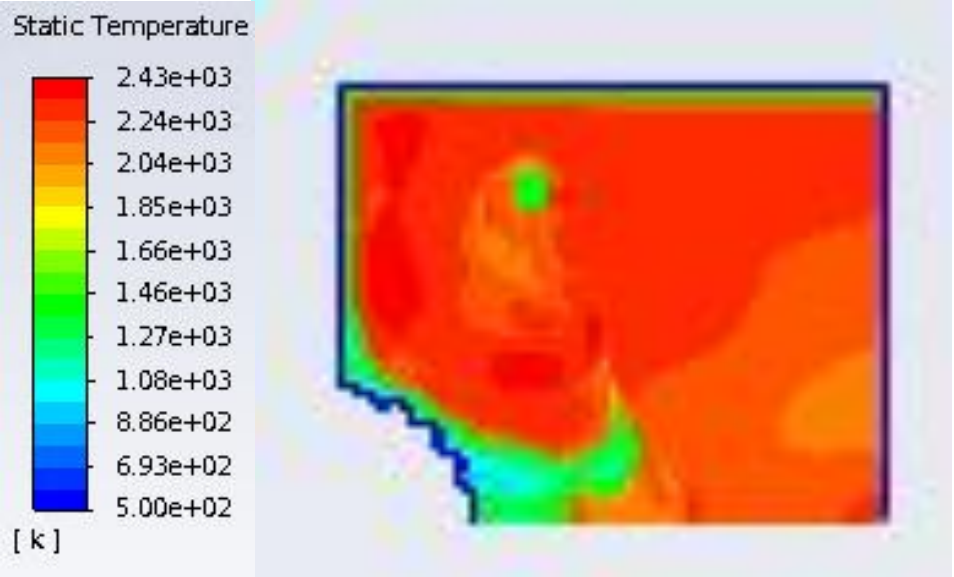

Figure 29: Thermal Contours of Golf Ball Case after Ignition

Similarities in the cold roll up structures seen in the baseline and golf ball cases pre-ignition carry over into the burn process. In both cases the far field region ignites with slight stratification and the cold gas reacts slowly. In both cases a clear cold roll up is apparent pre-ignition, and does not ignite with the bulk ignition. Similarly to the baseline case, the cold gas pockets progressively are heated, ignite and burn.

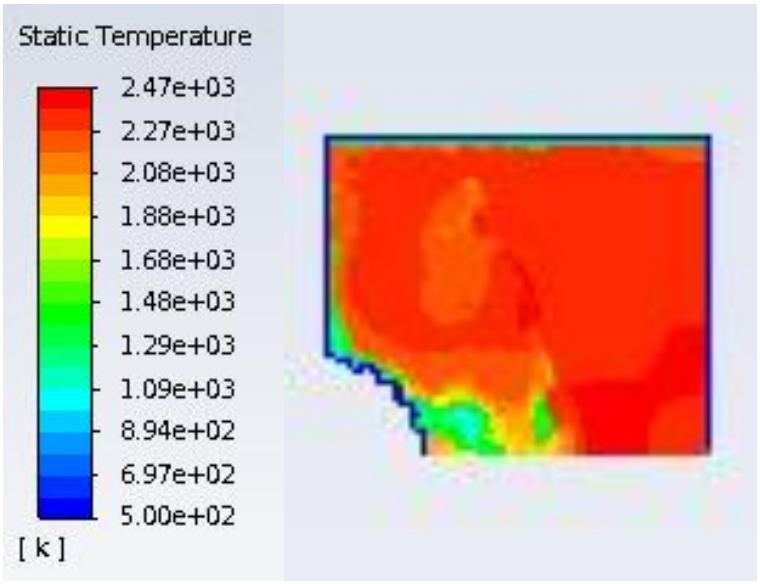
Static Temperature
2.47e+03
2.27e+03
2.08e+03
1.88e+03
1.68e+03
1.48e+03
1.29e+03
1.09e+03
8.94e+02
6.97e+02
5.00e+02
[k]

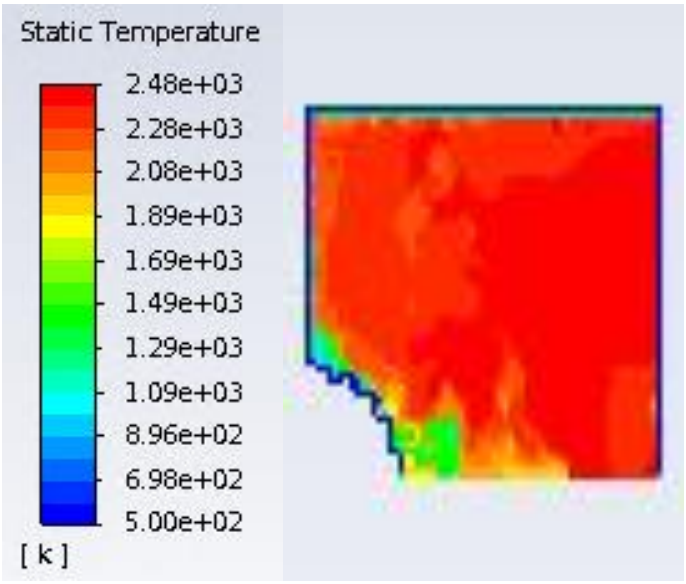
Static Temperature
2.48e+03
2.28e+03
2.08e+03
1.89e+03
1.69e+03
1.49e+03
1.29e+03
1.09e+03
8.96e+02
6.98e+02
5.00e+02
[k]

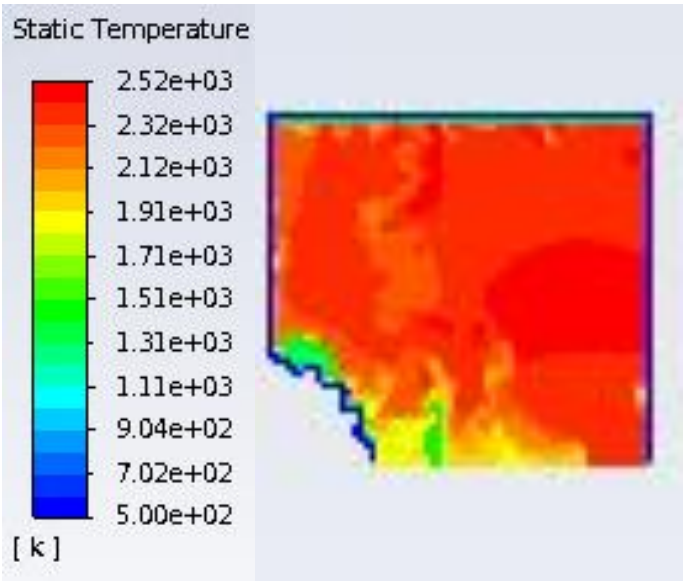
Static Temperature
2.52e+03
2.32e+03
2.12e+03
1.91e+03
1.71e+03
1.51e+03
1.31e+03
1.11e+03
9.04e+02
7.02e+02
5.00e+02
[k]

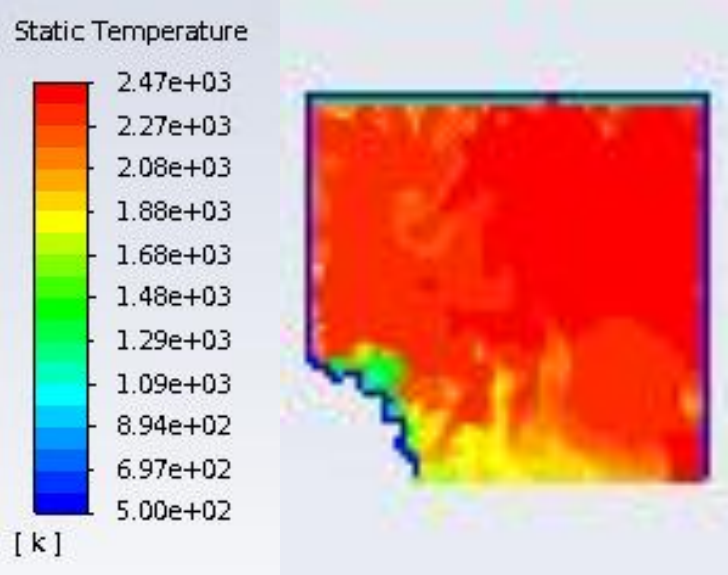

Figure 30: Golf Ball Case through Combustion, Starting t= 27.475 ms in 0.125 ms Increments

The golf ball case is different from the baseline case in that small pockets of gas are seen after ignition and react slowly. After the main ignition smaller cold gas vortices near the protrusion geometry are seen, and move towards the centerline due to a counter clockwise swirl in the domain. If droplet burning was applicable, smaller flow structures should have reacted rapidly, this is not the case. The smaller cold structures take longer to react than in the baseline case. This is likely due to the relative placement to other reaction zones. The warm pocket of air in the baseline case creates a buffer between the cold boundary condition and the cold vortex. This leads to warm products around the entire perimeter of the cold gas. In the golf ball case, the cold vortices are attachment to the cold boundary layer leading to an extended overall reaction.

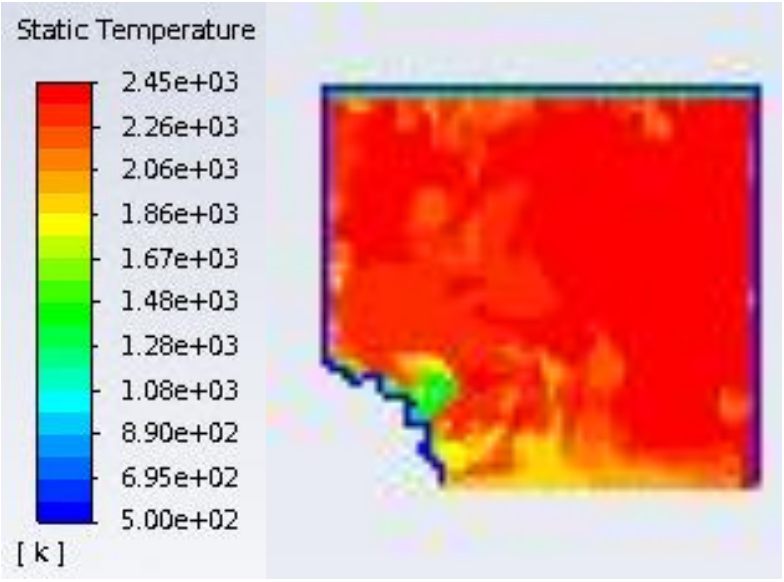
Static Temperature
2.45e+03
2.26e+03
2.06e+03
1.86e+03
1.67e+03
1.48e+03
1.28e+03
1.08e+03
8.90e+02
6.95e+02
5.00e+02
[k]

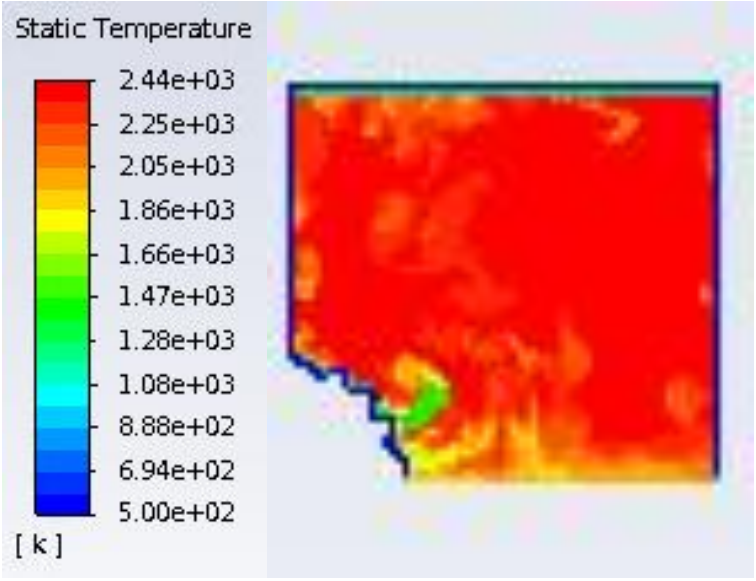
Static Temperature
2.44e+03
2.25e+03
2.05e+03
1.86e+03
1.66e+03
1.47e+03
1.28e+03
1.08e+03
8.88e+02
6.94e+02
5.00e+02
[k]

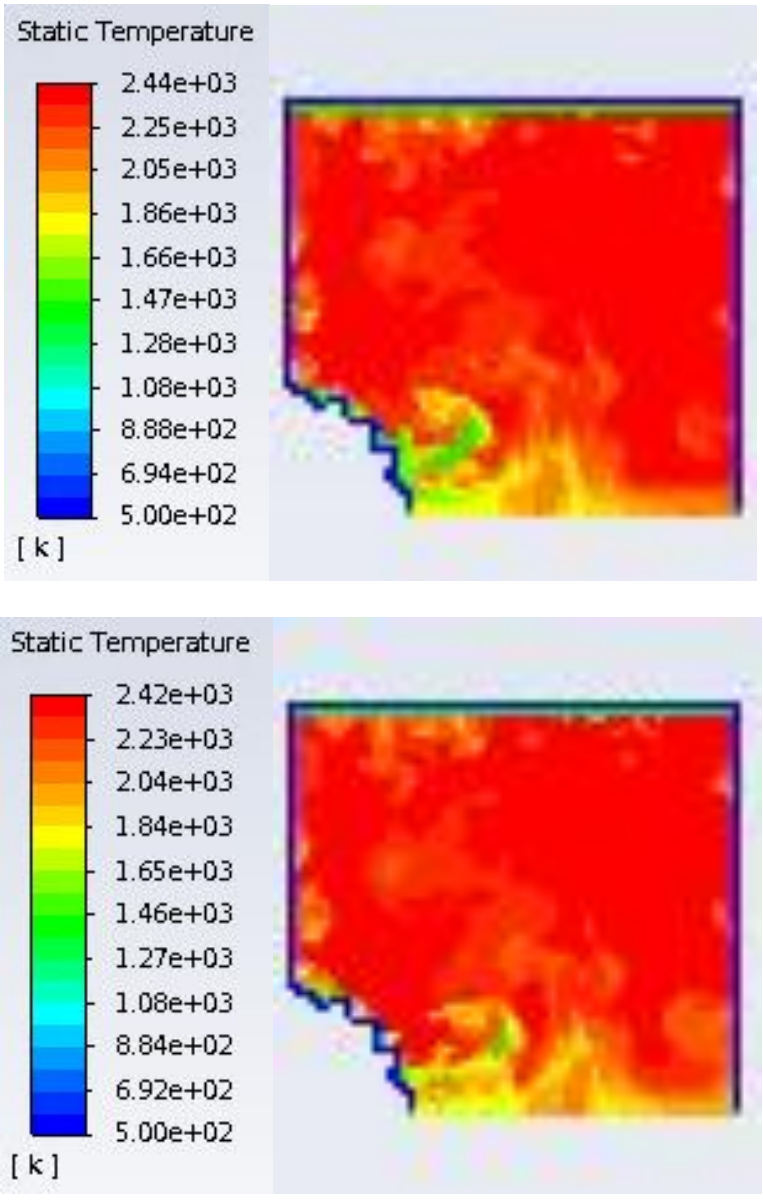

Figure 31: Golf Ball Case through Combustion, Starting t= 27.975 ms in 0.125 ms Increments

These lingering structures are bracketed by contours lasting 1.125 ms; a large increase over the baseline (0.75 ms) and ellipse (0.625 ms) cases to resolve the cold structures.

A majority of the intricacies of ignition, that are of interest in this work, occur between the pre and post ignition pictures however it would be computationally infeasible to increase the capture rate beyond what was used in these solves.

4.6 Turbulence Captured Near Walls

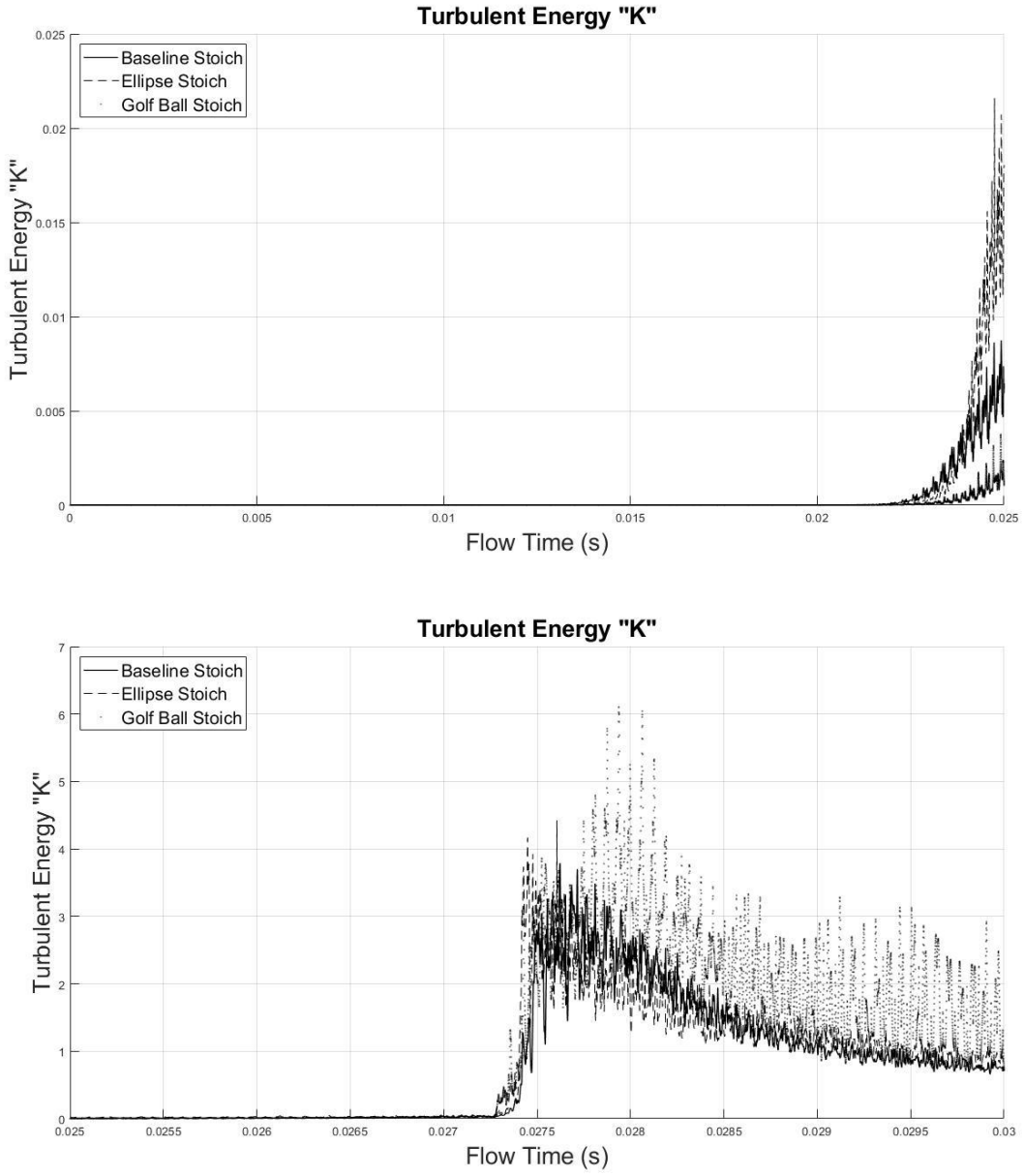

Figure 32: Turbulent K (m^2/s^2) through Compression (Top) and After (Bottom) vs Time (s)

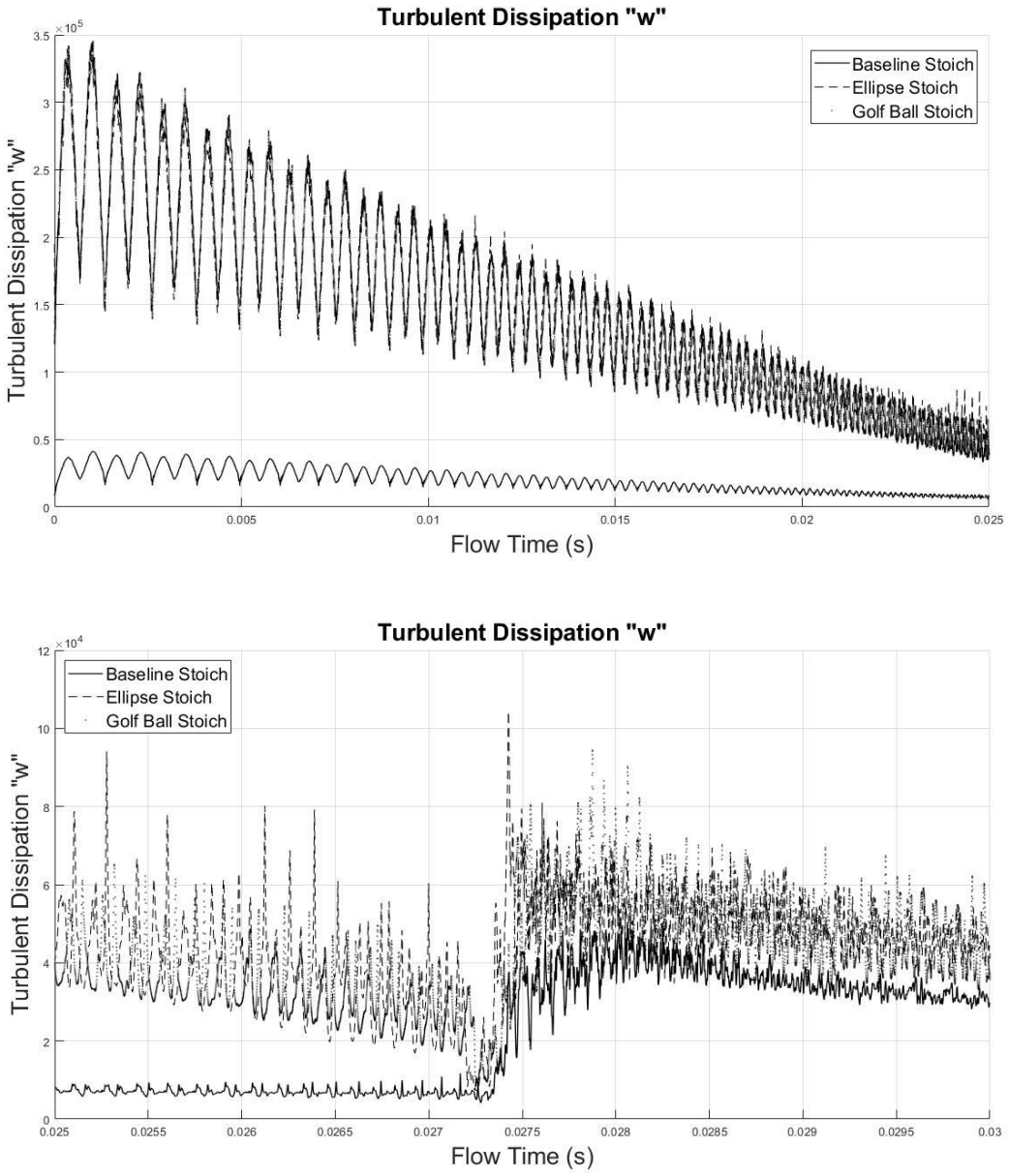

Figure 33: Turbulent Omega (s^{-1}) through Compression (Top) and After (Bottom) vs Time (s)

Turbulence at the wall is characterized with the RANS K-Omega Model, as discussed above. Assessing the mass averaged energy (K) terms vs time it is clear that there is little turbulence through compression for all cases. Across the board, after the large energy release associated with ignition a spike in energy is seen near the walls, Figure 32. As the gas swirls in

domain, shearing of the cold boundary layer around the problem would generate a good deal of turbulence.

The dissipation, Omega, monitor shows a differences between the baseline and complex geometries cases, possibly due to non-linear dissipation near the wall. The baseline case is different than the complex geometry studies through compression. This is perplexing since both the ellipse and golf ball cases have almost line on line agreement of turbulent diffusion however the qualitative compressions are quite different. This brings into question a difference in simulation time steps. As discussed above, to increase stability of the complex geometry cases started with a smaller time step, with more iterations. The complete alignment across all cases in the golf rollup generation from the piston / axial wall corner confirms initial time steps do not alter aerodynamic phenomena. The sustained elevated diffusion well after the initial few iteration also indicates this is not a contributor. An explanation could be turbulent flow structures' interaction with the cold boundary layer. If assumed linear, this would be proportional to the additional area due to the piston geometry. Since the additional area of the complex cases are not the same, baseline (3.142 in^2), golf ball (3.5196 in^2), ellipse (3.2116 in^2), so the dissipation must not be linear. This indicates the additional turbulence is generated and thus dissipated near the wall to produce the same levels of dissipation. The dissipation is high through compression while the energy is low indicating the model is quickly dampening turbulent structures. It is incredibly suspicious that the dissipation is line on line for the complex geometry cases, however do not seem to impact the cold roll up vortices studied in this paper.

4.7 Speciation History

This project looked to assess the detailed kinetic interaction with the cold roll up vortex. Assessing the global mass fraction of each case showed elevated level of long chain hydro-carbons prior to the main ignition. This finding is apparent by looking at the monitors in vs compression ratio.

The species were monitored through the study by outputting the molar fractions at each time step, mass fraction was synthesized in post processing. Due to the frequency of output and relative time scale vs the reaction time scale the monitors were condition to smooth out the signal and filter out numeric fluctuations. An assumed physical constraint is that decomposed should not reform, hence the mass fraction should never increase. To do this the n-heptane signal was averaged over an increasing size until the signal conformed to the idealized constraint. This means that the first derivative of conditioned signal using a centered stencil non-weighted rolling average should never be negative. Numeric fluctuations early in compression were ignored since the fuel was not decomposing and any changes were likely due to truncation error of the monitor, so only the first derivative after compression ratio greater than five was assessed. Since this filter artificially introduces diffusion some radicals which have short peaks during the reaction are smeared greatly and are likely sharper in time; since this is undesirable the smallest neighborhood reduces this as much as possible.

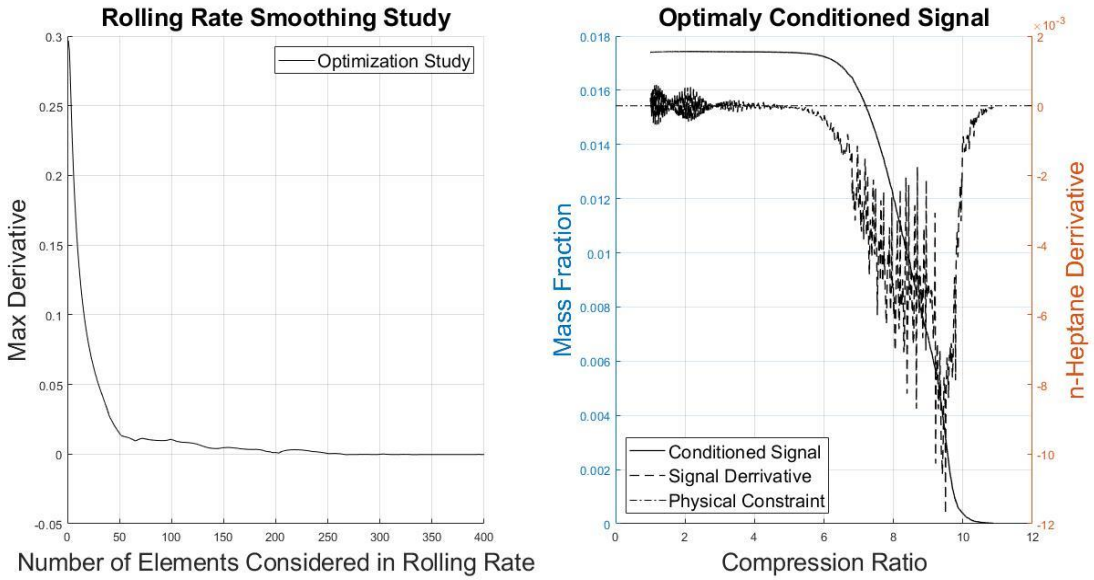

Figure 34: Heptane Mass Fraction Conditioning Study, Number of points in rolling average (Left) and Optimally Conditioned Signal w/ first Derivative (Right)

The left plot in Figure 34 show the max first derivative of the n-heptane mass fraction (for the CR of interest) vs size of neighborhood considered in the rolling average. The decreasing trend is aligned with the theory of the physical constraint. Ultimately an optimal filter considering 264 points prevents fuel reformation. This rolling average considers the monitor across 131 microseconds. The right plot of Figure 34 shows the optimally conditioned n-heptane monitor and confirms a negative derivative of the fuel through the reaction.

An additional quality check on the species monitor and mass fraction calculation was done through assessing the mass fractions of the inert species, Nitrogen and Argonne. Given there was no mechanism for Nitrogen or Argonne to decompose the mass fractions should remain constant throughout, while molar fractions can fluctuate. A flat monitor is seen in Figure 35, the max differences for Nitrogen of 0.03% and 0.5% for Argonne, deemed acceptable. The

elevated error for Argonne is expected as it was chosen as the unity species, so aggregates the numeric errors for all species.

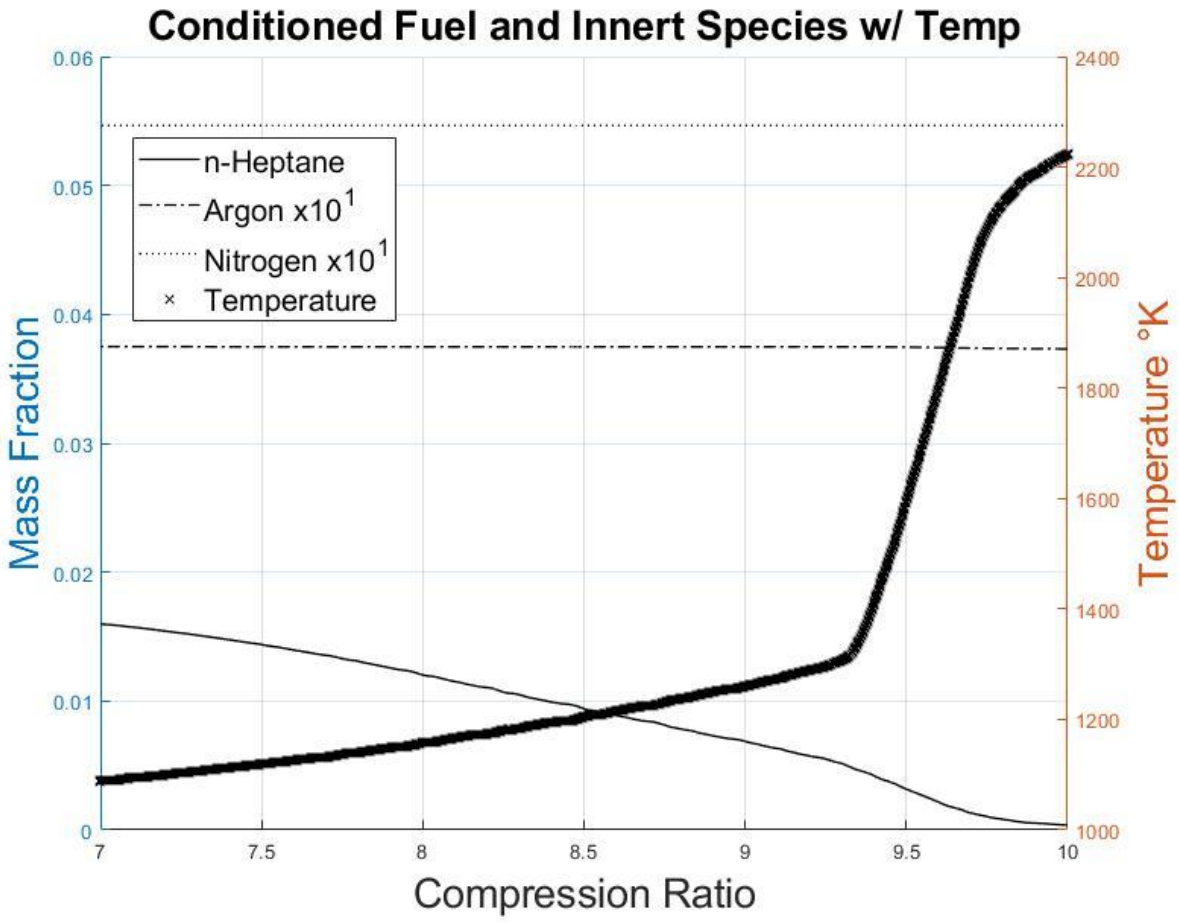

Figure 35: Baseline Mass Fraction of Conditioned Inert Species and Fuel Source

All species across the three cases are presented in Figure 36 for completeness.

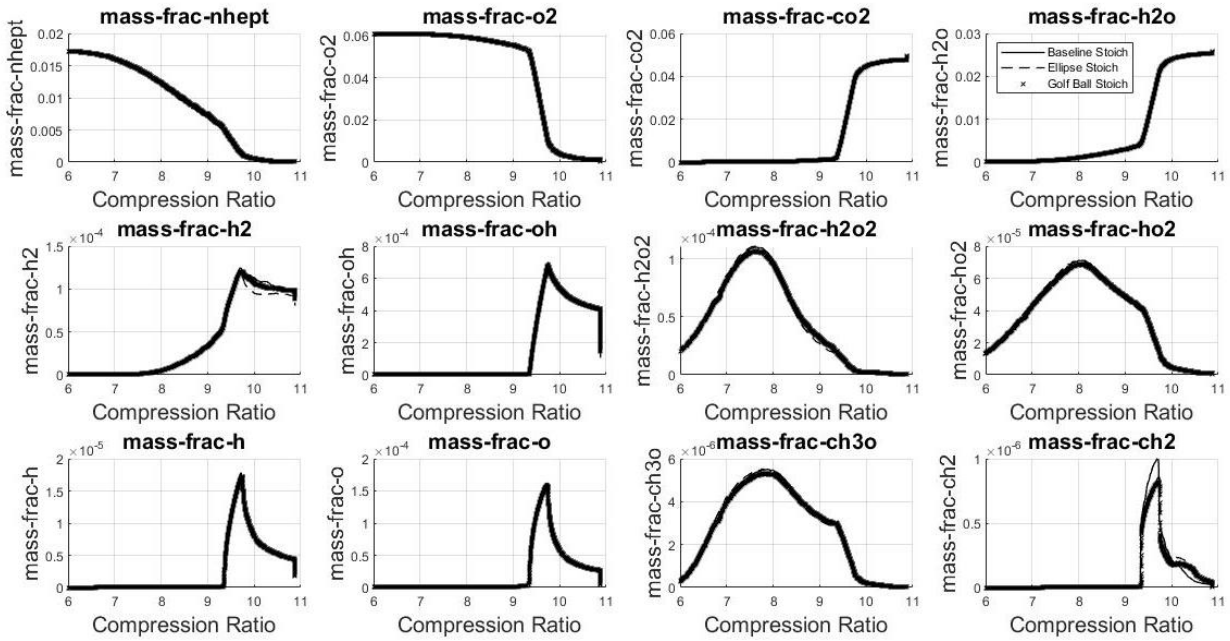

Figure 36: Conditioned Mass Fraction

Seen in Figure 36, there is a separation in H2 radicals between the ellipse case and the other two cases after the main ignition. The baseline CH2 monitor is an outlier during the main ignition compared to the other two cases. All other monitors are similar in shape and magnitude.

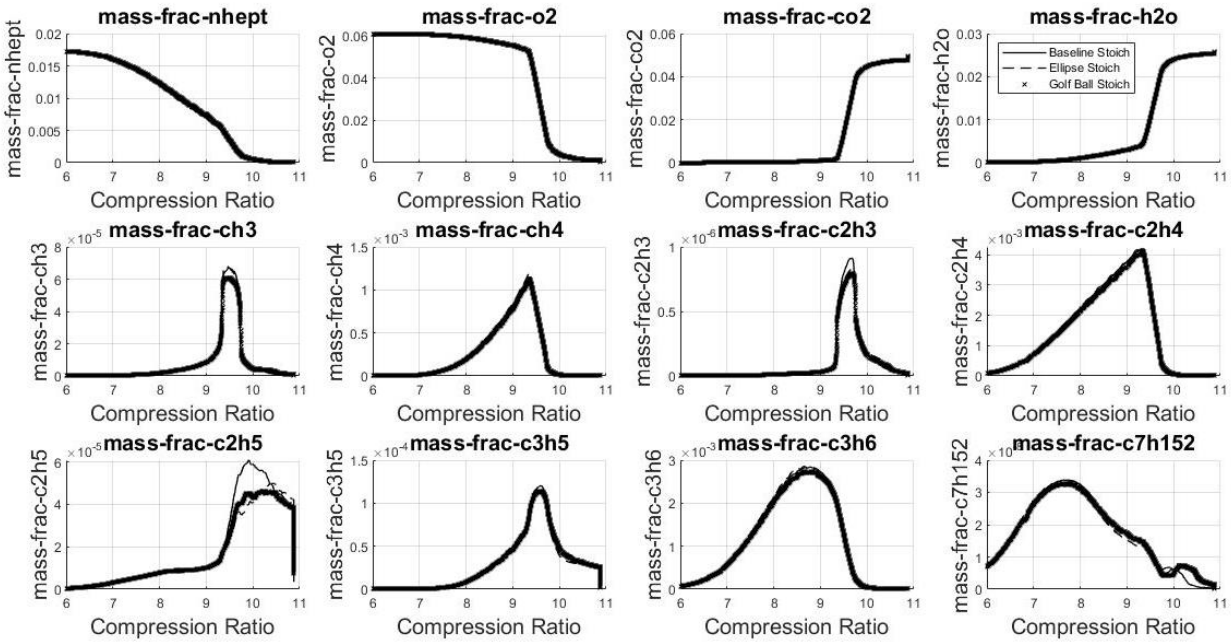

Figure 37: Conditioned Mass Fraction

Seen in Figure 37, a minor drop in methyl for the golf ball cases during the main ignition. An increase in both C2H3 and C2H5 for the baseline case during the main ignition compared to the other cases. Lastly a delayed offset of the ellipse and golf ball cases in a final bump of C7H15-2.

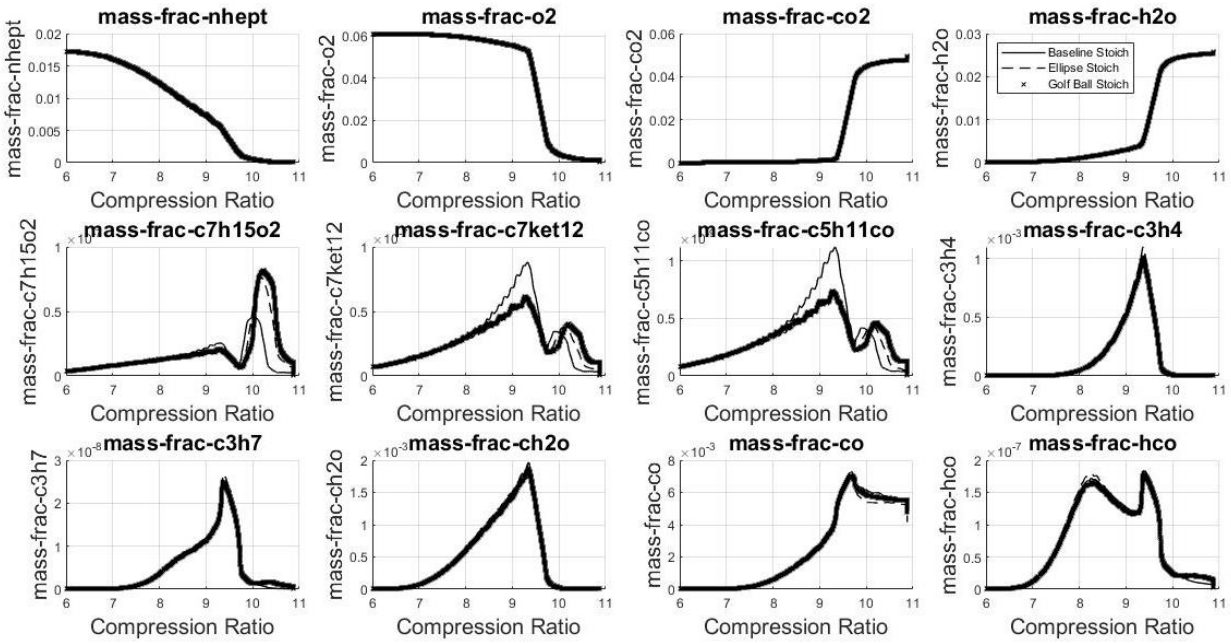

Figure 38: Conditioned Mass Fraction

Seen in Figure 38, a larger increase in C7KET12 and C5H11CO in the baseline case prior to ignition. An increased and delayed peak in C7H15O2 for the complex geometry cases after ignition. Stratified monitors for the main ignition (baseline and golf ball high, ellipse low) and HCO (baseline low, ellipse and golf ball high). These differences will assessed in further detail by the phase of occurrence, pre, during, and post the main ignition.

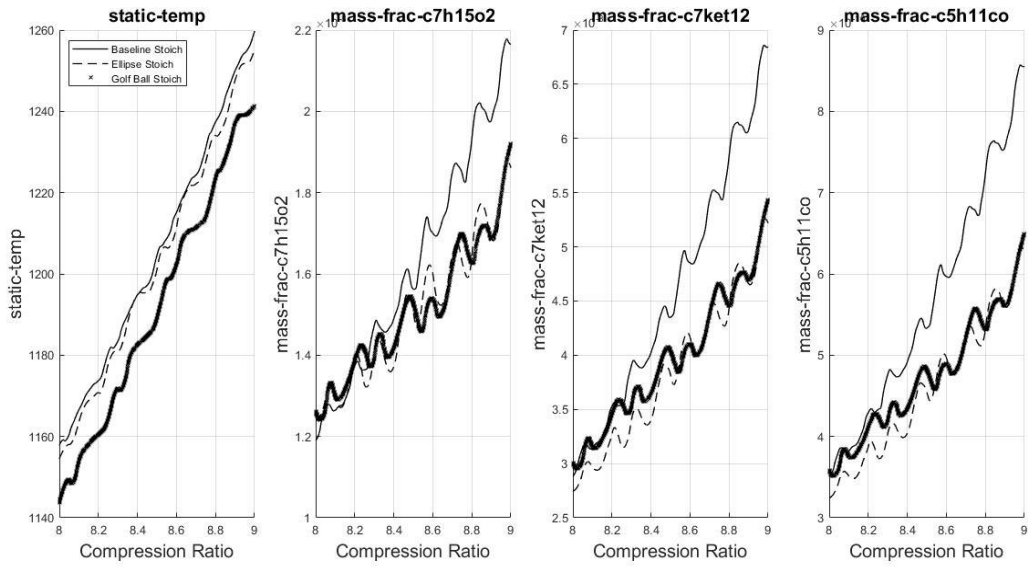

Figure 39: Conditioned Pre-Ignition Species of Interest vs Compression Ratio

Seen in Figure 39, before ignition the baseline case has elevated levels of large chain hydrocarbons.

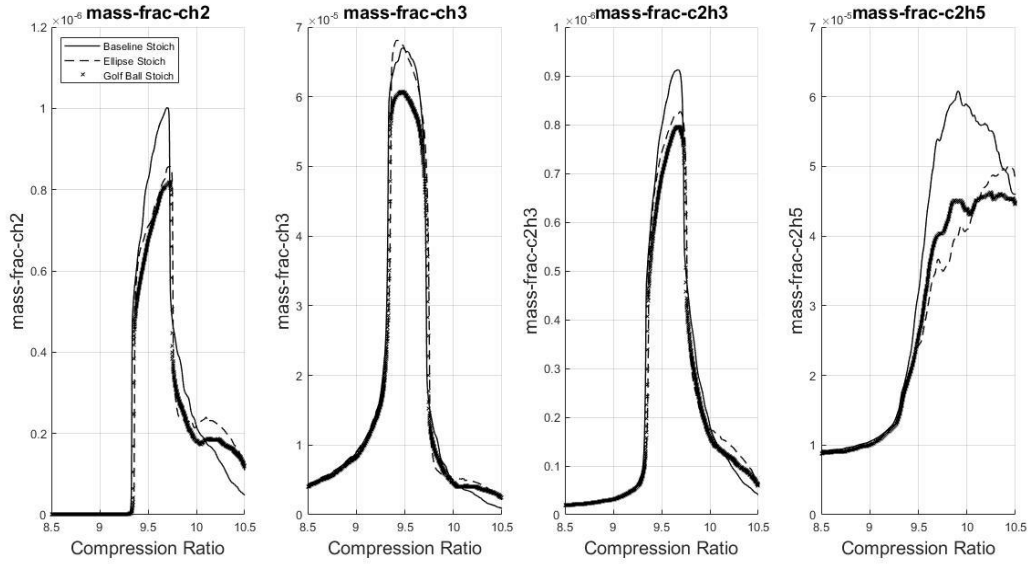

Figure 40: Conditioned Ignition Phase Species of Interest vs Compression Ratio

During ignition, the baseline case has elevated levels of CH2, C2H3, and C2H5, and the golf ball sees decreased levels of CH3 relative to the other two cases respectively.

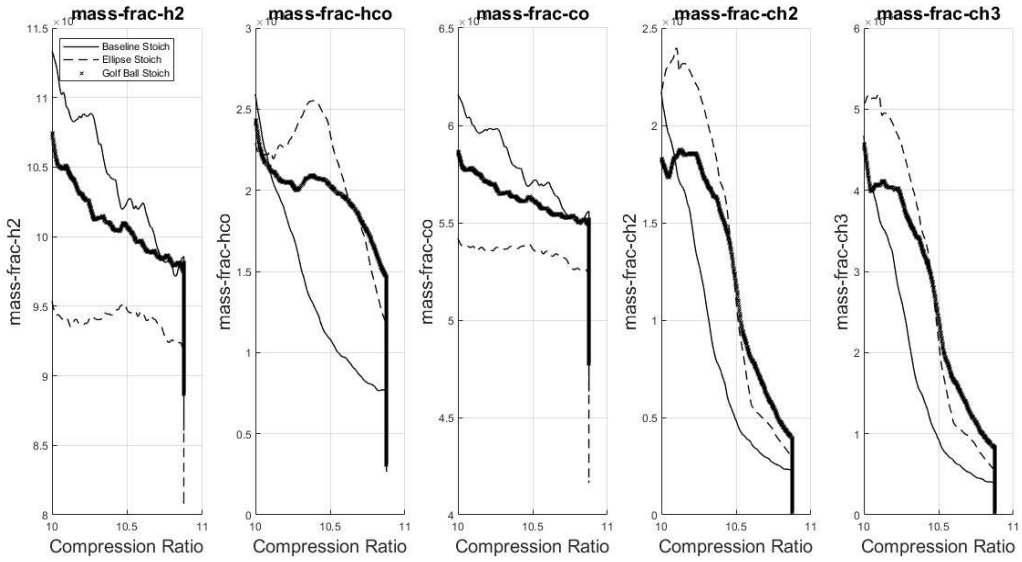

Figure 41: Conditioned Post Ignition Species of Interest vs Compression Ratio

The post ignition trend are stratified across the different cases due to late stage burning of the cold gas pockets and processing of reactants. Since the model was tuned and created to capture auto ignition, it is most accurate prior and during ignition. The model has obvious application flaws after the main reaction since it doesn't have nitrogen dissociation or other high temperature phenomenon.

Chapter 5: Discussion

5.1 Acoustic Signature and Reverberation

Thermal fluctuations seen in the global monitor were assessed and believed to be driven by acoustic phenomena in the gas domain. An acoustic wave is generated from the initial piston motion and the reverberation characteristics are highly sensitive to piston geometry. This is important as thermal fluctuations can be upwards of 50° K which can impact the kinetics. Further piston geometry manipulation and changes to the velocity profile would impact these fluctuation and alter the overall reaction.

Given the resolution of the mesh, numeric fluctuation likely have a physical interpretation. As discussed above the velocity oscillation were due to the expansion and compression of the acoustic wave propagating axially in the cylinder. To demonstrate this, the first derivative of the velocity monitor (proxy for acoustic wave) was compared against with thermal peaks for a segment of compression, seen in Figure 42. Note similar trends are observed for all of compression but requires zoom to see clearly.

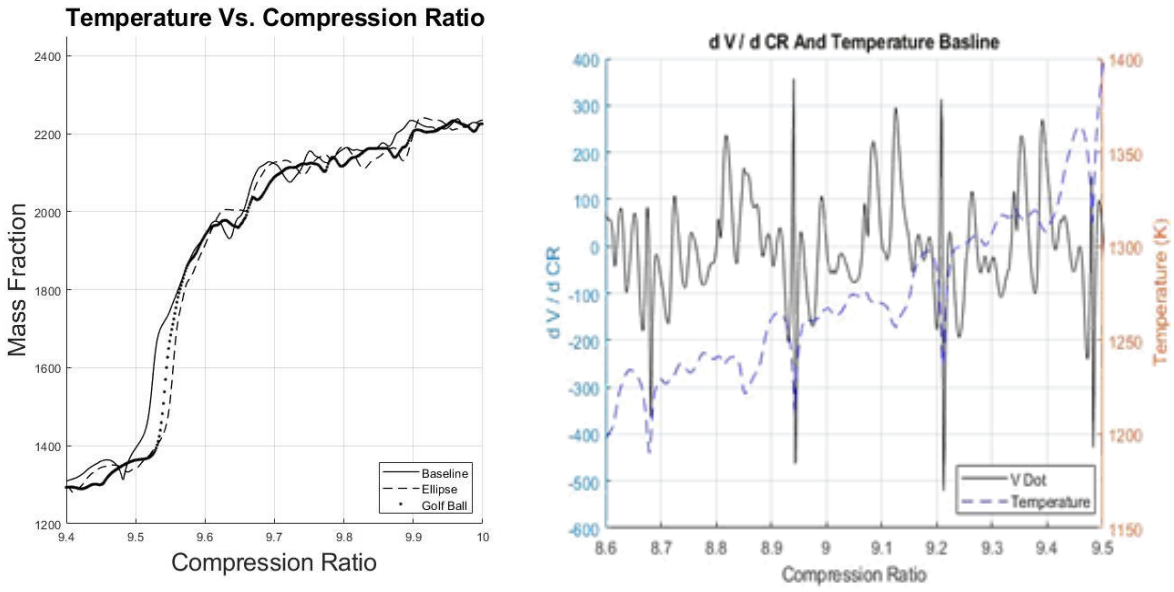

Figure 42: Temperature vs Compression Ratio of Interest (Left) and Velocity Derivative and Temperature vs Compression Ratio (Right)

When the acoustic wave, shown in Figure 11, is near either the top wall or piston most of the flow behind the wave is uniformly expanding. Once the wave reverberates on either boundary the compression wave dampens the fluid as it propagates back through the domain. This means there is a local maxima in the first derivative of the velocity monitor aligned with reverberation. This provides a correlations between the velocity derivative and the acoustic wave; hence the synthesized velocity derivative (V Dot) is a proxy for acoustics. Seen in Figure 42, the baseline case temperature dips have a strong correlation with blips of V Dot. What is also noticeable is the periodic oscillations between the clean V dot blips. It is proposed that the main clear blips signify the reverberation of the acoustic wave on the top domain of cylinder and the waves in the middle are the reverberation on the piston head. This could be impactful since these thermal divots can be up to 50° K which is large enough to alter the reaction mechanisms. This finding is impactful because if the acoustic waves could be actively dampened a more uniform thermal boundary could exist for studying the kinetics.

Since the speed of sound is temperature dependent, the size and shape of the cold roll up vortex would change the acoustic wave reverberation on the piston, especially when coupled with the ornate piston geometry. This idea was tested by looking at all the geometry cases and comparing the velocity derivative (V Dot) with the thermal derivative (T Dot). Assessing both derivatives, top plot in Figure 42, confirms correlation, however the interesting notes lie in the differences. The baseline case has the sharpest T dot and V dot; postulated to represent the reverberation on the top wall. The local maxima between the clear blips represents the wave reverberation on the piston. These diffusive spikes in V dot are due to the non-uniform aero-thermal structure in front of the piston.

In contrast, the golf ball V dot trace has a more diffusive structure. In the bottom plot of Figure 43, there are less sharp V dot blips, than those seen in the baseline case. As the wave reverberates on the golf ball's piston, the non-flat geometry produces a non-orthogonal reflection; this disperses the wave through time. Looking at the velocity and temperature derivatives near ignition the velocity derivative has only small blips and the temperature changes are more diffuse.

The ellipse case temperature and velocity derivatives are even more diffuse than the golf ball's, show in the middle plot of Figure 43. Velocity changes are much more sporadic consisting of reduced magnitude and less sharp definition. Earlier in time the velocity monitor is clearer but is dampened out closer to ignition, confirming the dispersion theory in time. This is believed to be due to the combination of a large cold region and piston protrusion of the ellipse case. The

ellipse case has the largest additional piston geometry and, seen in Figure 20, an expansive cold roll up vortex area though the gradient is less sharp.

The similarities of the baseline and golf ball are proposed to be due to the common flat regions of the piston, the baseline has a longer flat surface than the golf ball. The differences are due to the protrusion on the piston. The differences between the ellipse and the baseline is dampened out closer to ignition is due to the curved surface of the piston and the large cold gas region on the piston end of the domain. A possible flaw is if the temperature drives the acoustics, instead of the acoustics driving the temperature dips. While the two are connected, there is no mechanism for thermal oscillations without the acoustic wave. Temperature can be increased from work done by the piston, and can lose energy to the ambient.

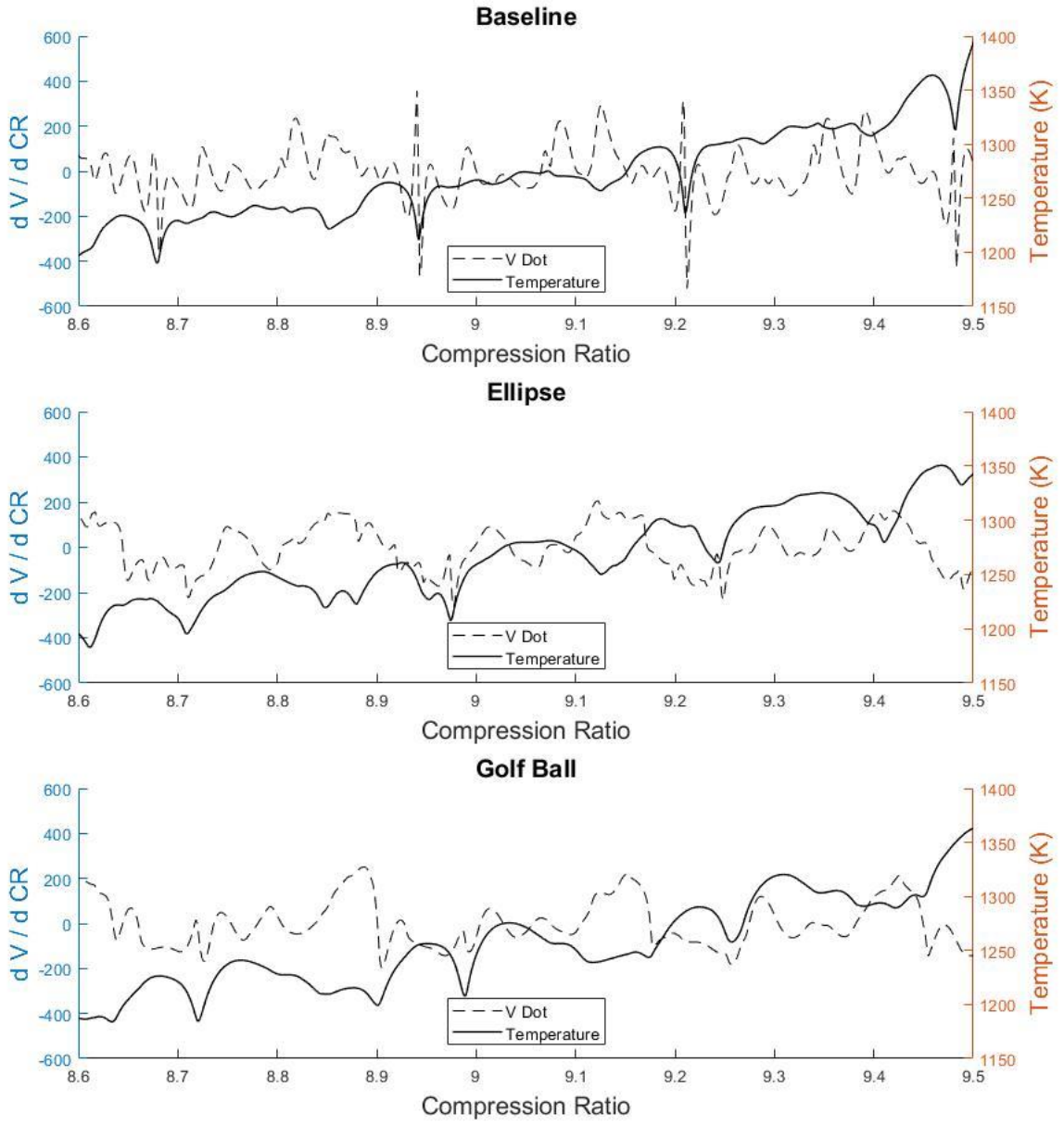

Figure 43: Temperature Derivative and Velocity Derivative vs Compression Ratio; All Cases

5.2 Low Temperature Chemistry

A major finding of this work was the elevated levels of long chain hydro-carbons indicating Low Temperature Chemistry (LTC) in the baseline case compared to both complex geometry cases. LTC is a specific fuel decomposition path which is an effective chain branching step at lower temperatures. Previous work indicates the effectiveness of accelerating ignition if LTC is leveraged. This work found the cold roll up vortex of the baseline case produces a large and clear cold region with a warm pocket in the heart of it which is postulated to greatly promote LTC.

LTC is one of two paths for n-heptane to decompose during chain branching and locally accelerates auto ignition. In the chemical kinetic model the initial decomposition of n-heptane has one path, and the secondary step has two pathways, Figure 44 shows the chain branching schematic.

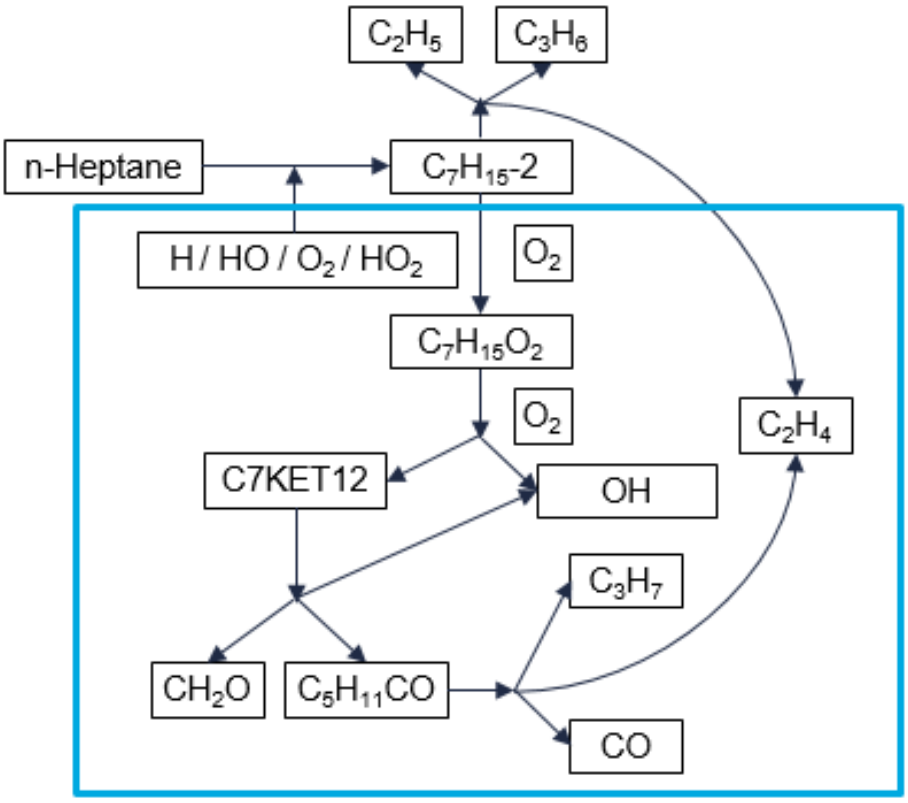

Figure 44: Chemical Model Chain Branching Pathway Schematic

The first step of the reaction mechanism involves n-heptane molecule losing a hydrogen atom to form C7H15-2; this is the only pathway to fuel decomposition so all molecules go through one of these 4 reactions. The decomposition of C7H15-2 has two pathways. Path 2A, shown in Equation 1, combines C7H15-2 with an O2 molecule to form C7H15O2. Path 2B, shown in Equation 2, allows C7H15-2 to decompose into three smaller hydrocarbon radicals.

$$C_7H_{15\_2} + O_2 \leftrightarrow C_7H_{15}O_2$$

Equation 1: Chain Branching Step 2A

$$C_7H_{15\_2} \leftrightarrow C_2H_5 + C_2H_4 + C_3H_6$$

Equation 2: Chain Branching Step 2B

An important component of the reaction pathway is the reaction rate constant modeled by Arrhenius's equation that control the reaction rate along with local species concentration. Local concentration will vary greatly through the solution. However for a premixed problem thermal gradients are generally larger than species gradients. This leads to reaction rate constants being a good indicator of the reaction. Arrhenius's equation is presented in Equation 3,

$$K = A\,T^{b}\,e^{-\frac{E_a}{RT}}$$

Equation 3: Arrhenius's Equation of Rate of Reaction Constant

With equation constants taken from the kinetic model show below in Table 3.

Table 3: Kinetic Model Reaction Rate Constants

Reac 1	Reac 2	Prod 1	Prod 2	Prod 3	A	B	Ea
C5H11CO		C2H4	C3H7	CO	9.84E+15	0	4.02E+04
C7H15-2	O2	C7H15O2			1.56E+12	0	0
C7H15-2		C2H5	C2H4	C3H6	7.05E+14	0	3.46E+04
C7H15O2	O2	C7KET12	OH		1.35E+14	0	18232.71
C7KET12		C5H11CO	CH2O	OH	3.53E+14	0	4.11E+04

With no initial energy input required for Path 2A, formation of C7H15O2 is possible at all temperatures and is driven by molar concentrations of C7H15-2 and Oxygen; hence the name Low Temperature Chemistry. Path 2B competes with LTC to break down C7H15-2, but has a high activation energy so is not prevalent at lower temperatures, assuming O2 molecules are present. Path 2B is highly temperature dependent because of the activation energy required. Path 2B has a higher pre-exponential factor (7.05 x 10^{14} mole-cm-sec-k) compared to Path 2A (1.56 x 10^{12} mole-cm-sec-k) which means that once the activation energy is overcome Path 2B is much

more prevalent. The trade off in reaction rates between of Path 2A and Path 2B vs temperature are see below in Figure 45.

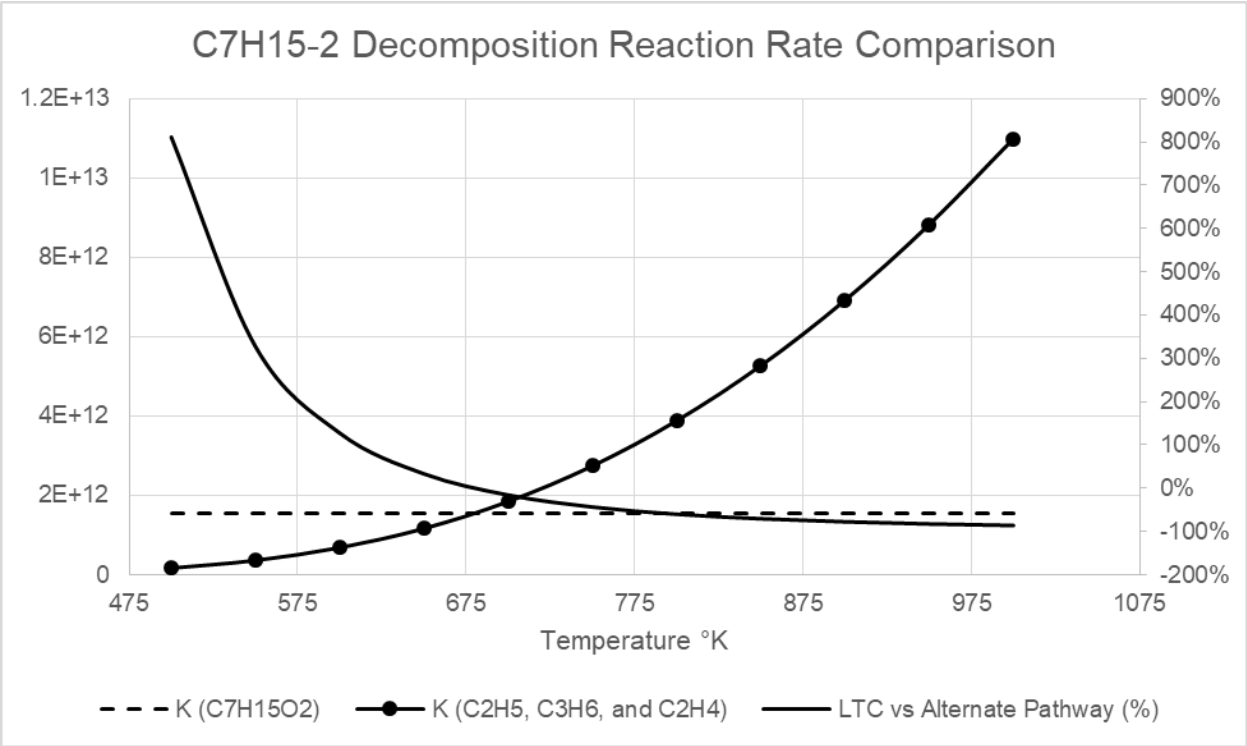

Figure 45: LTC and Alternate Reaction Pathway Reaction Rate (Left Y-Axis), Relative Comparison -- LTC vs Alternate Pathway (Right Y-Axis) vs Temp

Seen in Figure 45, the reaction rate is flat for Path 2A (dashed line) for all temperatures. Path 2B (Solid line with dot markers) is shown to be highly dependent upon temperature. The relative tradeoff (solid line) as a percentile comparison confirms the reduced prevalence on LTC at higher temperatures. This same effect is observed in Chemkin analysis where C7H15O2 is not present in solves with an initial temperature above 963° K.

LTC is the second chain branching step so requires an initial decomposition of n-heptane to provide the C7H15-2 radical. The first chain branching step, Path 1A-D occurs between the fuel source and H, OH, HO2, and O2, with activation energies 4760, 1090, 16950, and 47380 (cal/mole) respectively. This means n-heptane decomposition is more prevalent once H, OH, HO2 is present, but is reliant on decomposition with O2 to produce the smaller radicals.

Consider the initial fuel decomposition step 1D between n-heptane and Oxygen with Activation Energy of 47380 cal/mole and Path 2B with Activation Energy of 34600 cal/mole. If the environment is warm enough to overcome the energy required to decompose n-heptane it is also warm enough to promote Path 2B. This means that LTC is most likely to occur not where there are C7H15-2 can be produced through O2 decomposition of heptane, but where H, OH, HO2 radicals have diffused away from warmer regions to produce C7H15-2 radicals at lower temperatures.

LTC in an important mechanism in the study of auto ignition as it releases more energy than Path B sooner, accelerating chain branching and reduces the ignition delay. The reactions included in the LTC pathway, specifically C7Ket12, are key exothermic reactions early on in the mechanism [18]. While ultimately the same energy is released through either the high or low temperature pathway, the earlier the energy is released the faster the ignition can occur.

As shown above in Figure 39 the baseline case shows elevated levels of long chain hydro carbons such as C7H15O2, C7Ket12 and C5H11CO which are all constituents in the LTC pathway. The elevated monitors demonstrate increased utilization of the LTC pathway during

chain branching in the baseline case. Further, considering that the monitors are of global mass fraction, the local prevalence is likely higher. The much lower levels of C7H15O2, C7Ket12 and C5H11CO in the ellipse and golf ball case show the prevalence of the higher temperature pathway.

The increased prevalence of LTC in the baseline case is believed to be driven by the large cold roll up and enveloped warm pocket. This hypothesis is in agreement with optimal regions for LTC, discussed above, and illustrates why the baseline case sees LTC but the other cases do not. Under the assumption that LTC is prevalent in cold regions with radicals diffused from warmer regions, the increased utilization of LTC in the baseline case is reasonable. Shown in Figure 19, the baseline case has a clear cold roll up region but also has a warm perimeter and a warm pocket in the middle of the roll up. The inclusion of the warm pocket increases the amount of H, OH, HO2 radicals which decompose the n-heptane in LTC dominated regions.

The increased prevalence of LTC in the baseline case is due to an optimal environment for LTC whereas the ellipse has too much mixing, and the golf ball case's roll up is too small. The domain can be broken up into three regions, the cold boundary layer, the bulk flow and the cold roll up. In the boundary layer the temperature is too low (below 700°) to any chemical reaction until well after the bulk of the cylinder reacts. Intact the boundary layer remains intact until warm gas is mixed in well after ignition. The bulk of the gas in all cases is generally aligned with adiabatic compression and homogenous reaction. Thus, the differences in species across the cases must be tied to the roll up structures. Assessing the ellipse structure in Figure 20, the cold region is smaller and overall well mixed. Turbulent mixing would increase radical diffusion, but

also reduces the cold region by incorporating hot air having an overall net down force on LTC. Assessing the golf ball structures in Figure 21, a clear cold roll up (similar to the baseline case) exists but is smaller than the baseline and did not fold in a warm pocket as the baseline case did. The reduction in area and perimeter of the golf ball's roll up leads to a smaller region to see LTC.

A point of contention between the global monitors and the proposed LTC hypothesis is the lack of sensitivity. First, the increased utilization of LTC should have released more energy impacting the ignition delay, no meaningful difference in thermal monitors was observed. The second is an expected inverse thermal phenomenon proceeding ignition, which was not observed. Overall the global temperature is insensitive to any postulated chemical finding. As discussed above the increased use of LTC should have released more energy bringing forward the ignition. Shown above in Figure 23, there is a negligible difference in reaction timing. This is possibly due to the small scale on which the LTC mechanism was altered on and perhaps larger interaction and further reduced LTC would yield a larger impact on the reaction timing. One expected aspect of LTC is a global temperature drop before ignition, however was not apparent in these simulations. Since C7H15O2 formation is endothermic, an inverse temperature phenomenon is well document [27]. One explanation is the energy lost in the reaction is overcome by the work done through compression compensating for the bulk temperature. This phenomena would likely be more apparent if ignition occurs post compression. Overall the global temperature monitor may be a poor monitor for local thermal phenomenon. Given the postulated region where LTC occurs is small, the overall monitor may be artificially insensitive to the local thermal gradient.

One element of the project that could have boosted this finding is the inclusion of a local speciation monitor through the solution. This work presented the global monitor for each species however that reduces the opportunity to see local differences relative to the piston geometry. Furth work is proposed to consider this as an important aspect of this type of study. Specific opportunities for improvement would be either local monitors by discrete bodies of the domain or a spatial PDF of species monitors by cell.

Another aspect of the project that is worth further investigation is the sensitivity of the LTC finding due to reaction mechanism. LTC mechanisms can vary greatly across different reaction models so understanding the sensitivity of the LTC finding relative to the reaction mechanism would be interesting. Other models were considered for this work, however were not utilized to the extreme run time. As a proposal a single complex case and baseline case would be an interesting comparison for determining if there are differences related to the reaction mechanism.

The observed LTC utilization in the baseline case highlights the ability to impact the chemical kinetics through piston geometry. The speciation monitors show the increased prevalence of radicals which are found in the LTC pathway. The increase levels seen in only the baseline case indicates that inclusion of a variable piston head can alter the environment which promotes LTC. Assessing the contours provides possible flow structure elements that inhibit and promote LTC such as cold gas size and relative position to radical production.

5.3 Effect of Turbulence near Walls / Turbulent Chemistry Interaction

The effect of turbulence on the chemical reaction can be broken up by the two turbulence models used in the study, no numeric findings from the turbulence captured near the walls and the far field turbulence can be assessed qualitatively.

The RANS model was monitored through the solve by outputting the two constituents of the K-w model. As explained above, these two bulk parameters provide minimal information about the problem. The region of the problem that utilizes the RANS model is the small boundary layer around the exterior of the domain. The turbulent energy, and dissipation, are largely unchanged in compression. These monitors are only interesting once the bulk flow has reacted and the gas in the domain swirls shearing the boundary layer. No reaction is believed to be sustained in this region as the boundary condition dominates the temperature. Thus, regions resolved by K-w will have no direct impact on chemical kinetics or the larger reaction. This finding is aligned with the general lack of interesting findings in the results above.

The bulk of the RCM domain was well characterized through an LES model. These results clearly define the cold roll up and allow for the intricate investigation of aerodynamic structures generated in compression. Since LES numerically solves for large vortices, instead of modeling them as in RANS, extreme definition of aerodynamic structures was available which facilitated qualitative investigation of the flow. One deficit of this work is the lack of a quantitative monitor of the turbulence in this region, leaning instead on qualitative observations. While an explanation of why the baseline case had more LTC was presented above, a numeric

correlation is of interest. Additionally applying an LES model in 2D can be possibly misleading since LES is physically a 3D model. Turbulence is real terms is a 3D phenomenon and the application of LES aims to define the large turbulent structures precisely. By assessing only 2 dimensions special filtering is applied reducing the fidelity of the results. The nomenclature of this paper aligned with the Fluent's platform model usage to reduce ambiguity.

Turbulent chemistry is an important aspect of this work due to the inherent interaction of the cold roll up vortex and the chemical kinetics. Many TCI models exist in Fluent, such as laminar, Eddie Dissipation (EDM) and Eddy Dissipation Concept (EDC); which add additional levels of simulation to the reaction rates [23]. The laminar finite rate model which was used for this study only considers Arrhenius functions for chemical reaction rate, so does not add additional effects of turbulent fluctuations [23]. EDM places a floor on reaction rate and turbulence so forces an instant reaction wherever turbulent structures are present; EDM was not applicable to this problem. The EDC model allows for turbulent and chemical interaction by assessing the reaction in to the smallest turbulent scale [23]. This was believed to the ideal model since it was created to capture highly turbulent detailed chemical kinetics. As discussed in the model set up, the Fluent-Chemkin sub-problem found that using the EDC model forced TCI simulation and hampered the reaction; therefore not matching Chemkin results. A possible flaw in extrapolating the findings of the sub-problem to the full complex problem, is that the sub-problem did not have a lot of turbulence. If the EDC model does not handle laminar flows it could introduce numeric diffusion, this was not found in any literature. Furthermore it is assumed that TCI simulation is not required if both turbulence and chemical kinetics are well defined separately. Given the inclusion of detailed kinetics and an LES model it is likely only small

turbulent structures, which are filtered in LES, are not considered. This possible flaw could be further investigated by running concurrent models or comparison with experimental data.

5.4 Complex Geometry Impacts on Ignition

The additional piston geometry was shown to hamper LTC while having a minimal impact on the major species decomposition / formation or global thermal monitor. The ability to promote or dampen LTC bring the possibility of other kinetic pathways being manipulated by the cold roll up vortex.

Assessing the thermal monitor there is minimal change across the geometric cases. While some stratification is observed, the differences are small compared to the overall reaction time scale. It is assumed the reactions are nearly concurrent. Little change is seen in either the global fuel decomposition or the major product species, show in Figure 36. Alignment across the cases of temperature leading to alignment in global species monitor is expected. However, the altered reaction pathways through LTC discussed above demonstrate the differences due to the piston geometry.

As discussed above, elevated levels of long chain hydro-carbons indicate LTC in the baseline case compared to the complex geometry cases. The baseline case produced a large and clear cold region with a warm pocket in the middle which is postulated to promote LTC. The increased prevalence of LTC in the baseline case is due to an optimal environment for LTC whereas the ellipse has too much mixing, and the golf ball case's roll up is too small. This finding is aligned with previous work showing that the baseline case's cold roll up promotes

LTC but begins to probe at the specific flow characteristics of the rollup that are important and further impacts of altering the reaction pathways.

Demonstrated by the reduction in LTC, this work proposes possible manipulations to cold roll up vortex that can alter the reaction pathways. The piston geometry changes generated different flow structures in compression and impacted the chemical kinetics. This finding gives merit to the further study of piston geometry in attaining different kinetic reaction pathways. Possible outcomes include forcing reaction pathways that hamper emission formation.

While the ignition delays are roughly concurrent and occur within a small time scale relative to the reaction and flow time frame, the comparative reaction times are interesting and directly related to the aerodynamic structures generated by the piston. The golf ball geometry created a very coherent and attached roll up vortex which burned slowly. The elliptical geometry broke up the cold roll up vortex accelerating the reaction.

The golf ball case had an overall inefficient reaction. Lingering cold pockets seen long after the main ignition demonstrate the coherent cold roll up vortex leads to an extended combustion. Seen in Figure 31 small cold pockets remain long after the main ignition, increasing the overall reaction time to 1.125 ms, a 50% increase over the baseline case. This is interesting since the cold roll up structures in each case are similar. Both have clear triangular vortices prior to ignition. The golf ball case even has a smaller cold region so it is even more confounding that it burns slower. The important difference in the warm air pocket enveloped by the baseline case, which does not happen in the golf ball case. Without the warm air, the golf ball vortex burns

inefficiently. This is shown through a cold pocket that starts at the OD corner of the golf ball protrusion in Figure 30 and is sheared along the cold boundary in 30. It is then not surprising that this burns slowly as it is likely cooled by the boundary layer. In comparison, the baseline case does not have any cold pockets attached to the cold boundary layer; all cold vortex remnants are enveloped by warm gas post ignition so burn rapidly.

The ellipse case had the shortest overall reaction time. This was seen quantitatively to have highest Temperature derivative and qualitatively through the thermal contours. Shown in Figure 23, the peak ellipse temperature derivative was larger than the baseline and golf ball case's. The peak derivative implies that a large and even heat release occurred in this case. For a fixed amount of energy which can be released (mass of fuel was held constant for all cases) the faster the temperature rises the faster the overall reaction. Assessing the thermal contours qualitatively, in Figure 28, the reaction is bracketed (start / end) by the least number of framed indicating the fastest reaction The overall reaction bounds of 0.625 ms is a 17% reduction in reaction time compared to the baseline case (0.75 ms). This is driven by the well dispersed cold region after compression. As the cold roll up vortex interacts with the elliptical piston protrusion the structure begins to disperse. This yields many smaller flow structures but also mixed with warm air. Ultimately, prior to ignition more area is warmer and thus more likely to burn faster. This can be important for practical applications where peak work extraction vs time is of interest (such as engine timing). This work did not monitor pressure loading on the piston but would have been an interesting monitor of work timing.

The ellipse geometry providing an even reaction indicates geometry manipulation can mitigate the cold roll up vortex. If the cold roll up vortex could be completely diffused into the adiabatic region a homogenous temperature profile may be obtained. Currently near homogenous thermal flow is attained through crevice implementation, however crevices do not capture the roll up completely and have issues containing the captured flow. A piston protrusion might be easier to implement in a test set up as the complexities are in manufacturing not configuration. Complex geometries are more difficult to manufacture than a flat piston, however the ellipse case is likely more achievable than the golf ball and is a common piston shape in industry. Unlike implementing a crevice, diffusing the roll up would increase turbulence which is not ideal for non-turbulent kinetic study. However, introducing turbulence would facilitate detailed studies of coupled turbulent kinetic problems.

Chapter 6: Conclusion

2D axisymmetric CFD RCM simulations leveraging detailed chemical kinetics and refined flow were used to study the effect of piston geometry on ignition delay. The three geometries of interest were unique shapes that were targeted to either break up the main roll up vortex or generate new roll ups. The detailed chemical kinetics used a reduced global mechanism for n-heptane built to model ignition in a HCCI engine. The finite fluid structures were resolved with a hybrid RANS – LES model.

Negligible difference in ignition delay across the variable pistons was seen, however chain branching mechanisms, specifically LTC, were greatly impacted by the piston geometry. The baseline case saw high levels of LTC as a result of the cold roll up vortex growing and enveloping warm air during compression. The ellipse case did not see high levels of LTC but saw a well-mixed gas domain leading to a short total reaction time. The golf ball case saw an intricate cold roll up vortex and did not see high levels of LTC. The golf ball case highlights the impact of the warm air pocket in the baseline case as both cases have a similar vortex structure but the golf ball does not have a warm air pocket. A strong correlation was found in the temperature and velocity derivative, leading to a discussion of acoustic reverberation. Piston geometry and the cold rollup vortex is believed to have an impact on the acoustic reverberation characteristics of waves generated in compression; which can impact the global temperature fluctuations in the gas domain.

The ability to promote or dampen LTC bring the possibility of other kinetic pathways being manipulated by the cold roll up vortex. This confirms previous finding that the cold roll up

promotes LTC but begins to probe at the specific flow characteristics of the rollup that drive LTC pathways. Discussed above, the enveloping of a warm gas pocket in the vortex, and the large volume of cold gas promotes LTC in the baseline case. Both the ellipse and golf ball case altered the roll up vortex and thus dampened LTC. The ellipse broke up the optimal LTC environment by dispersing the cold region. The golf ball altered the volume and warm air enveloped by the cold roll up.

Demonstrated by the reduction in LTC, this work proposes possible manipulations to cold roll up vortex that can alter the reaction pathways. The vortex break up and mixing seen in the ellipse case proposes the possibility of vortex mitigation through piston geometry. In many RCM investigations the cold roll up vortex is captured to provide a homogenous field for kinetic study. Given various difficulties completely capturing the vortex using a crevice, a variable piston may be easier to implement. This work confirms merit in the ability to alter the flow field and reaction pathways by changing the piston head. Possible deficiencies in the model were the lack of turbulent monitors for the LES region and not including TCI in the volumetric reaction model. The finding of LTC was heavily dependent upon global monitors of mass fraction, however could have been supported further through local speciation or a finer understanding of species distribution. Since LTC mechanisms can vary greatly between models, it would be interesting to understand the sensitivity of the LTC finding through assessing other reaction mechanisms. Further work to investigate the turbulence interaction and assess different fuel ratios and fuel sources would be interesting next steps. Shape optimization and possible combination with crevice technology could provide better control of experiments.

Chapter 7: Future Work

This work was able to study the cold roll up vortex and how geometric features could impact the structure. Further work utilizing the model could be done to find numeric correlations between the turbulence and kinetics, leverage different reaction models, assess different fuels and fuel levels, and optimal configuration of geometry and piston geometry are possible next steps. The first improvement for future work is a numeric monitor assessment of the turbulent structures that would allow a numeric based assessment of the impact of the vortices on the chemical kinetics and thus reaction. This work presented qualitative results for the non-boundary layer flow but lacked a run monitor for numeric characterization. The volumetric reaction model could be changed. The decision to model no TCI was made based ground work to match a CFD model to Chemkin results. While this allowed for assurance that the model aligned with Chemkin, it simplifies many of the complexities of the larger problem. Possible mitigation through ensuring the model is mesh insensitive could have indicated if TCI simulation was needed. Further assessment in relation to test data would capture proper model application. The proposed work outlined a plan to assess different fuel types and understand the effects across different fuel ratios, these runs were simulated however have not been post processed; this would be a topic likely included future work. The ellipse case found to be the most promising shape to break up the cold roll up vortex and further investigation different elliptical key points would be key to attempting to break up and thoroughly mix the problem. The finding of alternate reaction path ways could be looked at further by optimizing the geometry to drive larger change in the species levels. Further work to probe the sensitivity of the LTC findings to the kinetic model chosen would be interesting. Lastly, combining previous work of crevice implementation and some piston protrusion might be interesting as producing an optimal field for kinematic studies.

REFERENCES

[1] W. Leary, E. S. Taylor and C. F. Taylor, "A Rapid Compression Machine Suitable for Studying Short Ignition Delays (NACA-TN-1332)," National Advisory Committee for Aeronautics, Washington, DC, 1945.

[2] C.-J. Sung and H. J. Curran, "Using rapid compression machines for chemical kinetics studies," *Progress In Energy And Combustion Science,* vol. 44, pp. 1-18, 2014.

[3] H. Daneshyar, D. E. Fuller and B. E. L. Deckker, "Vortex Motion Induced By The Piston Of An Internal Combustion Engine," *International Journal of Mechanical Sciences,* vol. 15, no. 5, pp. 381-386, 1973.

[4] S. Frolov, M. Emans, V. Ivanov, B. Basara, V. Leshevich and O. Penyazkov, "3D simulation of hydrogen ignition in a rapid compression machine," *Journal of Loss Prevention in the Process Industries,* vol. 26, pp. 1558-1568, 2013.

[5] J. F. GRIFFITHS, Q. JIAO, a. W. K. M. SCHREIBER and a. K. F. K. J. MEYER, "Experimental and Numerical Studies of Ditertiary Butyl Peroxide Combustion at High Pressures in a Rapid Compression Machine," *COMBUSTION AND FLAME,* vol. 93, pp. 303-315, 1993.

[6] K. Chen, G. Karim and H. Watson, "Experimental and Analytical Examination of the Development of Inhomogeneities and Autoignition During Rapid Compression of HydrogenOxygen-Argon Mixtures," *Journal of Engineering for Gas Turbines and Power,* vol. 125, no. 2, pp. 458-465, 2003.

[7] S. H. G. V. M. S. W. H. J. C. C.-J. S. Scott Goldsborough, "Advances in rapid compression machine studies of low and intermediate-temperature autoignition phenomena," *Progress in Energy and Combustion Science,* vol. 63, pp. 1-78, 2017.

[8] P. Park and J. Keck, "Rapid compression machine measurements of ignition delays," 1990.

[9] D. Lee and S. Hochgreb, "Rapid Compression Machines: Heat Transfer and Suppression of Corner Vortex," *Combustion and Flame,* vol. 114, no. 3, pp. 531-545, 1998.

[10] G. Mittal and S. Gupta, "Computational assessment of an approach for implementing," *Fuel,* pp. 536-544, 2012.

[11] G. Mittal and C.-J. Sung, "Aerodynamics inside a rapid compression machine," *Combustion and Flame,* vol. 145, pp. 160-180, 2006.

[12] J. Wurmel and J. Simmie, "CFD studies of a twin-piston rapid compression machine," *Combustion and Flame,* vol. 141, p. 417–430, 2005.

[13] G. Mittal and A. Bhari, "A rapid compression machine with crevice containment," *Combustion and Flame,* vol. 160, no. 12, pp. 2975-2981, 2013.

[14] H. Yerrennagoudarua and K. Manjunatha, "Combustion analysis of modified inverted “M” type piston for diesel engine with platinum coating and without coating by using CFD," *Materials Today,* vol. 4, p. 2333–2340, 2017.

[15] K. Ravi, J. P. Bhasker, J. Alexander and E. Porpatham, "CFD study and experimental investigation of piston geometry induced incylinder," *Fuel,* vol. 213, p. 1–11, 2018.

[16] B. Harshavardhan and J. Mallikarjuna, "Effect of piston shape on in-cylinder flows and airefuel interaction in a direct injection spark ignition engine e A CFD analysis," *Energy*, vol. 81, pp. 361-372, 2015.

[17] R. J. Kee, F. M. Rupley and J. A. Miller, "Chemkin-II: A Fortran chemical kinetics package for the analysis of gas-phase chemical kinetics," United States, 1989.

[18] A. Patel, S.-C. Kong and R. D. Reitz, "Development and Validation of a Reduced Reaction Mechanism for HCCI Engine Simulations," *SAE TECHNICAL Reprint; Homogeneous Charge Compression Ignition (HCCI) Combustion*, 2004.

[19] A. E. Lutz, R. J. Kee and J. A. Miller, "SENKIN: A Fortran program for predicting homogeneous gas phase chemical kinetics with sensitivity analysis," United States, 1988.

[20] M. Mehl, W. Pitz, C. Westbrook and H. Curran, "Kinetic Modeling of Gasoline Surrogate Components and Mixtures Under Engine Conditions," *Proceedings of the Combustion Institute*, vol. 33, pp. 193-200 , 2011.

[21] C. S. Yoo, T. Lu, J. H. Chenc and C. Law, "Direct numerical simulations of ignition of a lean n-heptane/air mixture with temperature inhomogeneities at constant volume: Parametric study," *Combustion and Flame*, vol. 158, no. 9, pp. 1727-1741, 2011.

[22] S. R. Turns, An Introduction To Combustion: Concepts and Applications, New York, NY: McGraw hill, 2011.

[23] ANSYS, *ANSYS FLUENT 12.0 Theory Guide*, Canonsburg, PA, 2009.

[24] R. H. Pletcher, J. C. Tannehill and D. A. Anderson, Computational Fluid Mechanics and Heat Transfer, Boca Raton, FL: CRC Press, 2013.

[25] M. Ihme, "On the role of turbulence and compositional fluctuations in rapid," *Combustion and Flame*, vol. 159, pp. 1592-1604, 2012.

[26] Q.-h. Luo, J.-B. Hu, B.-g. Sun, F.-s. Liu, X. Wang, C. Li and L.-z. Bao, "Experimental investigation of combustion characteristics and NOx emission of a turbocharged hydrogen internal combustion engine," *International Journal of Hydrogen Energy*, vol. 44, pp. 5573-5584, 2019.

[27] U. C. MULLER and N. PETERS, "GLOBAL KINETICS FOR n-HEPTANE IGNITION AT HIGH PRESSURES," in *Twenty-Fourth Symposium (International) on Combustion*, 1992.

[28] T. Lu and C. K. Law, "A criterion based on computational singular perturbation for the identification of quasi steady state species: A reduced mechanism for methane oxidation with NO chemistry," *Combustion and Flame*, vol. 154, pp. 761-774, 2008.